










RESEARCH ARTICLE

The spinal muscular atrophy gene product regulates actin dynamics

Tobias Schüning^{1,2}  | Andre Zeug³  | Katharina Strienke^{1,2}  | Peter Franz⁴  |
 Georgios Tsiavaliaris⁴  | Niko Hensel²  | Gabriella Viero⁵  |
 Evgeni Ponimaskin²  | Peter Claus^{1,6,7} 

¹SMATHERIA gGmbH – Non-Profit Biomedical Research Institute, Hannover, Germany

²Department of Anatomy and Cell Biology, Faculty of Medicine, Martin Luther University Halle-Wittenberg, Halle (Saale), Germany

³Institute of Cellular Neurophysiology, Hannover Medical School, Hannover, Germany

⁴Cellular Biophysics, Institute for Biophysical Chemistry, Hannover Medical School, Hannover, Germany

⁵Institute of Biophysics (IBF), CNR Unit at Trento, Trento, Italy

⁶Center for Systems Neuroscience (ZSN), Hannover, Germany

⁷Institute of Functional and Applied Anatomy, Hannover Medical School, Hannover, Germany

Correspondence

Peter Claus, SMATHERIA gGmbH – Non-Profit Biomedical Research Institute, Feodor-Lynen-Str. 31, D-30625 Hannover, Germany.
 Email: peter.claus@smatheria.org, claus.peter@mh-hannover.de

Funding information

Deutsche Forschungsgemeinschaft (DFG), Grant/Award Number: PO732 and ZE994; European Research Council (ERC), Grant/Award Number: 956185; Konrad-Adenauer-Stiftung (KAS)

Abstract

Spinal Muscular Atrophy (SMA) is a neuromuscular disease caused by low levels of the Survival of Motoneuron (SMN) protein. SMN interacts with and regulates the actin-binding protein profilin2a, thereby influencing actin dynamics. Dysfunctional actin dynamics caused by SMN loss disrupts neurite outgrowth, axonal pathfinding, and formation of functional synapses in neurons. Whether the SMN protein directly interacts with and regulates filamentous (F-) and monomeric globular (G-) actin is still elusive. In a quantitative single cell approach, we show that SMN loss leads to dysregulated F-/G-actin fractions. Furthermore, quantitative assessment of cell morphology suggests an F-actin organizational defect. Interestingly, this is mediated by an interaction of SMN with G- and F-actin. In co-immunoprecipitation, in-vitro pulldown and co-localization assays, we elucidated that this interaction is independent of the SMN-profilin2a interaction. Therefore, we suggest two populations being relevant for functional actin dynamics in healthy neurons: SMN-profilin2a-actin and SMN-actin. Additionally, those two populations may influence each other and therefore regulate binding of SMN to actin. In SMA, we showed a dysregulated co-localization pattern of SMN-actin which could only partially be rescued by SMN restoration. However, dysregulation of F-/G-actin fractions was reduced by SMN restoration. Taken together, our results suggest a novel molecular function of SMN in binding to actin independent from SMN-profilin2a interaction.

KEYWORDS

actin, actin dynamics, profilin2a, spinal muscular atrophy (SMA), Survival of Motoneuron (SMN) protein

Abbreviations: CNV, copy number variation; F-actin, filamentous actin; G-actin, globular actin; GST, Glutathione-S-transferase; PFN2a, profilin 2a; PLP, poly-L-proline; SMA, spinal muscular atrophy; SMN, survival of motoneuron; WT, wild-type.

This is an open access article under the terms of the [Creative Commons Attribution-NonCommercial-NoDerivs](https://creativecommons.org/licenses/by-nc-nd/4.0/) License, which permits use and distribution in any medium, provided the original work is properly cited, the use is non-commercial and no modifications or adaptations are made.

© 2024 The Author(s). *The FASEB Journal* published by Wiley Periodicals LLC on behalf of Federation of American Societies for Experimental Biology.

1 | INTRODUCTION

Spinal Muscular Atrophy (SMA) is an autosomal recessive neurodegenerative disease predominantly affecting children. SMA manifests in severe proximal muscular atrophy due to a progressive loss of alpha motoneurons in the ventral horn of the spinal cord and the brain stem. In addition, SMA is characterized as a multi-system disorder since neuronal and non-neuronal tissues are affected.^{1–13} The cause of SMA is the homozygous loss or mutation of the Survival Motoneuron 1 (*SMN1*) gene encoding the ubiquitously expressed Survival of Motoneuron (SMN) protein.^{14,15} Humans harbor a homologous gene (*SMN2*). However, due to a critical mutation of *SMN2*, its expression results predominantly in a truncated and instable SMN isoform (SMN Δ 7). Therefore, *SMN2* cannot compensate the loss of *SMN1*. Nevertheless, a higher copy number (copy number variation, CNV) of *SMN2* leads to increased protein levels and can ameliorate SMA severity.^{16–20} Accordingly, five classical SMA subtypes ranging from types 0 to V were classified based on symptoms like age of onset and achieved motor milestones.^{21–23}

First successful therapeutic strategies target the rescue of SMN protein levels by different mechanisms. Nusinersen corrects the *SMN2* pre-mRNA splicing by enhancing inclusion of exon 7, thereby increasing full-length SMN protein expression.²⁴ Risdiplam is a small molecule, which acts in a similar way on the *SMN2* pre-mRNA splicing with a different mode of administration.²⁵ Onasemnogene abeparvovec is a gene replacement therapy and uses an AAV9 vector for delivering the SMN cDNA.²⁶ Although these therapeutic options represent undoubtedly milestones in disease treatment, all of them lack the full capacity to restore SMN functions in the whole system of the body and in all types of SMA. Moreover, all treatment options focus on restoration of SMN protein levels which may not correct degenerative processes that have already become SMN-irreversible by the intervention timepoint. Thus, available treatment options are not necessarily capable of rescuing dysregulated molecular pathways and functions.²⁷ Pathways regulated by the SMN protein can be a target for SMN-independent combinatorial approaches. Therefore, elucidating protein–protein interactions and regulatory switches of the SMN protein might contribute to understand cellular dysregulations in SMA.

SMN localizes to the cytoplasm and to the nucleus. Nuclear import relies on the formation of the SMN complex²⁸ which has essential functions involving biogenesis and assembly of *small nuclear ribonucleoproteins* (snRNPs),^{29–31} pre-mRNA splicing,³² DNA repair³³ and R-loop resolution.^{34,35} In motoneurons, SMN is involved in the development of neuromuscular junctions (NMJs),^{36,37} proprioceptive synapses and functional sensory motor circuits.^{38–40} SMN also regulates synaptic signaling and

endocytosis of synaptic vesicles.⁴¹ Additionally, we and others showed that SMN loss causes a dysregulation of neurite outgrowth^{42,43} and neurotrophic signaling pathways.^{44–48} Neuronal development involves axonal pathfinding, synapse formation and cytoskeletal dynamics. One essential part of the cytoskeleton is actin.^{49,50} The actin cytoskeleton is a highly dynamic system of monomeric, globular (G-) actin and filamentous (F-) actin. The equilibrium between these states is tightly regulated by different actin-binding proteins, which are relevant for polymerization of G-actin into F-actin or for depolymerization of F-actin filaments.⁴⁹ Interestingly, SMN regulates actin dynamics by a direct interaction via its poly-L-proline (PLP) stretch to the actin-binding protein profilin2a (PFN2a).^{51–53} Profilins are small proteins with binding sites for G-actin, phosphatidylinositol 4,5-bisphosphate (PIP2) and poly-L-proline (PLP) binding domains.^{49,54} An interactor of profilins is the Ena/VASP-complex which is essential for F-actin elongation in developing neurons.⁵⁴ However, profilins are tightly regulated in vivo by Rho-associated protein kinase (ROCK).⁵⁵

SMN loss causes disruption of its binding to PFN2a and has detrimental consequences also on other targets downstream of ROCK such as cofilin and myosin-light chain phosphatase.^{45,52} These dysregulations lead to altered actin dynamics, as quantified by calculations of F-/G-actin ratios or fractions. We showed in growth cones of SMA motoneurons, that F-/G-actin ratios are shifted compared to control motoneurons leading to growth cone collapse.⁵² Taken together, these results suggest a dysregulation of the homeostasis of the actin cytoskeleton in SMN-depleted cells, due to the loss of SMN-dependent regulatory effects on actin-binding proteins. However, whether the SMN protein directly interacts with the actin cytoskeleton is still an open question. SMN may either stabilize actin directly or contribute to filament formation as shown by in vitro polymerization assays.⁵⁶

In this study, we aim at analyzing the consequences of SMN loss in neuronal morphology as caused by alterations of actin dynamics. We elucidated how the SMN protein is regulating actin dynamics. SMN co-localized in vivo with and directly bound in vitro to both G- and F-actin, but preferentially with and to G-actin. Furthermore, we showed that the co-localization is independent of SMN-profilin2a binding. Our results suggest the existence of two populations of SMN associated with actin in neurons: SMN-PFN2a-actin and SMN-actin are both influencing each other and are relevant for functional actin dynamics. In SMA, we report defects in the balance of the residual SMN binding to G- and F-actin, with SMN more co-localizing with F-actin. Full restoration of SMN protein levels could not completely rescue this imbalance, however, corrected the shift of increased F-/G-actin fractions upon SMN loss.

2 | MATERIALS AND METHODS

2.1 | Cell culture and transfection

Motoneuron-like NSC34 cells (murine neuroblastoma x spinal cord hybrid cell line⁵⁷) were incubated at 37°C in a humidified atmosphere with 5% CO₂. NSC34 cells were cultivated in proliferation medium (Dulbecco's Modified Eagle's Medium (DMEM) with GlutaMAX-I supplemented with 5% Fetal Bovine Serum (FBS), 100 U mL⁻¹ penicillin and 0.1 mg/mL streptomycin) and cells were split every 3–4 days. Cells were seeded for experiments on day in vitro 1 (DIV1) in proliferation medium. At DIV2, media was changed to FBS-reduced starvation media (DMEM with GlutaMAX-I supplemented with 1% FBS, 100 × U mL⁻¹ penicillin and 0.1 mg/mL streptomycin) and cells were transfected using Lipofectamine2000 according to the manufacturer's instructions (Thermo Fisher Scientific, Carlsbad, USA). After 6 h of transfection, cells were incubated with differentiation media (DMEM with GlutaMAX-I supplemented with 1% FBS, 1 μM all-trans retinoic acid, 100 U mL⁻¹ penicillin and 0.1 mg/mL streptomycin) to increase dendrite formation of NSC34 cells. At DIV4, cells were harvested for further analysis.

2.2 | Plasmids and site-directed mutagenesis

Cloning of human SMN cDNA into the pEGFP-N2 vector was described previously.^{42,52} Here, the EGFP-tag of the SMN construct was exchanged to a Flag-tag at the C-terminus using the following primers: ND35_EcoRI_hSMN_pEGFP-N2_FP (5'-TCA AGC TTC GAA TTC ATG ATG GCG ATG-3'), ND49_SalI_STOP_Flag_hSMN_pEGFP-N2_RP (5'- A CGC GTC GAC TTA CTT ATC GTC GTC GTC CTT GTA ATC ATT TAA GGA ATG TGA GCA C-3'). The PCR for insert amplification was conducted using Pfu DNA Polymerase (Promega, #M7741, Germany) and cloned into the pCI-neo-Vector (Promega, #E1841, Germany) via EcoRI and SalI restriction sites. Synthesis of the pCI-neo-SMN-S230L-Flag construct was conducted via site-directed mutagenesis using the following primers: (5'-CCACTTACTATTATGCTGGCTG-3') and (5'-CAGCCAGCATAATAGTAAGTGG-3') with Pfu DNA Polymerase used for amplification. All inserts were completely sequenced. Plasmid preparation for transfection assays was performed using Qiagen Plasmid Maxi Kit (Qiagen, #12162, Germany) according to the manufacturer's instructions (Qiagen, Hilden, Germany).

2.3 | Protein purification of SMN-GST and actin

E. coli strain BL21 (DE3) was transformed with pET41a-GST-SMN⁵⁸ and grown in 250 mL 2× LB to OD₆₀₀ of 0.6–0.8. SMN-GST expression was induced by adding 1 mM IPTG [Neofroxx, #1122GR005] for 6 h at 37°C. Cells were harvested by centrifugation, frozen at –20°C, thawed and resuspended in lysis buffer (10 mM Tris [pH 8.0], 1 mM EDTA, 2 mM DTT) supplemented with 1× cComplete™ Protease Inhibitor Cocktail [Roche, #04693132001] and 1 mg/mL Lysozyme [NeoFroxx, #1256GR001]. After 30 min incubation on ice, cells were sonicated and lysate was clarified by centrifugation at 10 000 × rcf for 30 min followed by incubation at room temperature for 30 min with GST Bind™ Resin [Novagen, #70541-3], which was preequilibrated with lysis buffer.

Purified chicken muscle G-actin was prepared as described previously.⁵⁹ Actin polymerization was induced by adding 50 mM KCl and 2 mM MgCl₂ followed by incubation for 1 h at room temperature. F-actin was pelleted by centrifugation at 55 000 rpm (Beckman Coulter, TLA-55) and was reconstituted in RIPA buffer (20 mM Tris [pH 7.5], 137 mM NaCl, 25 mM β-glycerophosphate, 2 mM EDTA, 1% (v/v) Tergitol, 1% (w/v) Sodium Deoxycholate).

2.4 | Cell lysis and Western Blot Analysis

For Western Blot Analysis of SMN protein levels in different CRISPR/CAS-modified NSC34 cells,⁶⁰ 300 000 cells were seeded in a 6-well format on DIV1. After 24 h, media was changed to starvation media for transfection or directly to differentiation media. After 6 h of transfection, starvation media was exchanged to differentiation media. Cells were differentiated to DIV5, washed with PBS and lysed with RIPA buffer (20 mM Tris-HCl pH 7.5, 137 mM NaCl, 25 mM β-Glycerophosphate, 2 mM EDTA, 1% Tergitol (v/v), 1% Desoxycholate (w/v), 1× cComplete™ Protease Inhibitor Cocktail [Roche, #04693132001], 1× PhosSTOP™ [Roche, #04906837001]). Suspension was incubated for 20 min on ice followed by 20 min centrifugation at 21 000 × rcf, 4°C. Supernatant was collected in a fresh reaction tube and protein concentration was determined using the bicinchoninic acid (BCA) assay. 30 μg of total protein per sample was used for sodium dodecylsulfate polyacrylamide gel electrophoresis (SDS-PAGE) and Western Blot Analysis. After blotting on nitrocellulose (NC) membrane (Cytiva, Amersham™ Protran™ #10600003), Ponceau S staining was performed for detection of total protein. Membranes were destained and blocked with 5% (w/v) dry milk in Tris-buffered saline with 0.1% (v/v) Tween20 (TBS-T) for

20 min and incubated with α -SMN antibody (monoclonal, 1:1000, BD Transduction Laboratories, #610647) or α -DYKDDDD-tag (Flag-tag) antibody (monoclonal, 1:5000, Proteintech, #66008-4-Ig) overnight at 4°C. Next day, membrane was incubated with secondary HRP labeled antibody (ECL α -Mouse IgG HRP linked with whole antibody, Amersham #NA931V or ECL α -Rabbit IgG HRP linked F(ab')₂ fragment, Amersham #NA9340V) for 1 h at room temperature (RT) in 5% (w/v) dry milk in TBS-T and detected with chemiluminescence (Immobilon® Western Chemiluminescent HRP Substrate, Millipore #WBKLS0500) on an INTAS imager (Intas, Göttingen, Germany).

2.5 | Immunoprecipitation

300 000 cells were seeded at DIV1 in 6-well format in proliferation medium. On DIV2, either transfection of cells in starvation medium and change to differentiation medium after 6 h of transfection was performed or direct change to differentiation medium, respectively. Cells were lysed with RIPA buffer at DIV5 as described above. 150 μ g of total protein was transferred into a new reaction tube and 1 μ g of primary antibody, (see above for α -SMN and α -DYKDDDD-tag, α -actin (monoclonal, 1:1000, Abcam, #ab179467)) was added and incubated on a rotating shaker overnight at 4°C. Dynabeads™ Protein G (Invitrogen, #10003D) were washed once with PBS, pre-blocked with 0.5% BSA for 1 h at RT on a rotating shaker, washed again once with PBS, and once with RIPA and resuspended in RIPA. The beads were added to the protein lysate and primary antibodies, incubated for 1 h on a rotating shaker at RT. Supernatant was collected as a control for SDS-PAGE and afterwards beads were washed three times with RIPA and once with PBS. Before eluting proteins from the beads with 25 μ L of 1 \times Laemmli Buffer, bead suspension was transferred to a new reaction tube to omit contamination with unspecific proteins bound to the surface of tubes. Proteins in Laemmli buffer were heated to 95°C for 10 min before running an SDS-PAGE and a Western-Blot analysis (see above). Detection of proteins was done as described above with depicted antibodies α -SMN or α -Actin.

2.6 | In vitro pulldown assay of SMN-GST and actin

SMN-bound beads were blocked for 30 min at room temperature with RIPA buffer supplemented with 0.5% (w/v) BSA prior to addition of either G-actin in G-buffer (5 mM Tris-HCl [pH 8.0], 0.1 mM CaCl₂, 0.2 mM ATP [Roche, #10127523001], 0.5 mM DTT), G-actin: Latrunculin B

[Merck, #L5288] (Ratio 1:2) in G-buffer, or F-actin in RIPA buffer. Mixtures were incubated for 60 min at 4°C. The resin was washed twice with RIPA buffer, three times with PBS and finally incubated with 1 \times Laemmli buffer for 5 min at 95°C. Samples were further processed by Western-Blot analysis. Detection of SMN and actin on NC membrane was performed as described above.

2.7 | Immunocytochemistry

Glass cover slips in 24 wells were incubated with poly-L-proline (PLL) (0.221166 mg/mL) at least for 30 min at 37°C, 5%CO₂ in a humidified atmosphere. Cover slips were washed afterwards two times with Ampuwa rinsing solution (Fresenius Kabi, #B230672) and once with proliferation medium. 30 000 cells were seeded on DIV1 on glass cover slips covered with 0.5 mL proliferation medium. On DIV2, either transfection was performed as described or medium was directly switched to differentiation medium. On DIV5, cells were fixed with 4%PFA in PBS for 10 min at RT. Cells were washed 3x with appropriate volume of PBS. For F-/G-actin staining, cells were permeabilized with 1% Albumin bovine serum (BSA) (w/v), 1%Tergitol in PBS for 15 min at RT. After PBS washing, cells were incubated either with 1 μ g/mL Phalloidin-Tetramethylrhodamin B-Isothiocyant (Sigma, #P1951) or Alexa Fluor™ Plus 555 Phalloidin (Invitrogen, #A30106) and 12 μ g/mL Deoxyribonuclease I, Alexa Flour™ 488 Conjugate (Invitrogen, #D12371) in 1% BSA(w/v) in PBS for 30 min at RT. After extensive washing, cover slips were mounted with ProLong™ Diamond Antifade mountant (Invitrogen, #P36970) or labeled with a primary antibody (see above for α -SMN & α -DYKDDDD-tag, followed by DAPI (neoFroxx, #1322MG005) staining). For SMN or DYKDDDD-tag, cells were permeabilized and blocked with 5% Normal Goat Serum (NGS), 0.3% Tergitol (v/v) in PBS for 1 h followed by incubation in 1% NGS, 0.3% Tergitol (v/v), α -SMN or α -DYKDDDD-tag overnight at 4°C. For profilin2 staining, cells were blocked and permeabilized with 5% Horse Serum (HS), 1% Tergitol (v/v) in PBS for 10 min followed by incubation with α -PFN2 (1:1000, Sigma #P0101) in 1% HS, 0.3% Tergitol (v/v) in PBS. For Y12 staining, cells were permeabilized with 5% NGS, 1% Tergitol (v/v) in PBS for 10 min RT, followed by 30 min blocking with 1% NGS, 1% Tergitol (v/v) in PBS and staining overnight at 4°C with α -Smith antigen [Y12] (1:250, Abcam #ab3138) in 1% NGS, 0.3% Tergitol (v/v) in PBS. For Gemin2 staining, cells were permeabilized with 5%NGS, 1%Tergitol(v/v) in PBS for 10 min RT followed by 60 min blocking in 1%NGS, 1%Tergitol(v/v) in PBS and staining overnight at 4°C with α -Gemin2 [2E17] (1:1000, Merck #05-1540) in 1% NGS, 0.3% Tergitol (v/v)

in PBS. All fluorescently labeled secondary antibodies were stained for 1 h at RT in 1% NGS/0.3% Tergitol (v/v) in PBS. Antibodies used were goat α -mouse IgG (H+L) Alexa Flour™ 488 (1:500, Invitrogen #A-11029), goat α -mouse IgG (H+L) Alexa Flour™ 647 (1:500, Invitrogen #A-21235), goat α -rabbit IgG (H+L) Alexa Flour™ 555 (1:500, Invitrogen #A-21429). All cover slips for co-localization analysis were stained with DAPI for 5 min at RT directly before mounting with ProLong™ Diamond Antifade mountant (Invitrogen, #P36970). Microscopy was done 24 h after mounting cover slips on the microscope slides.

2.8 | Microscopy and image analysis

All images were acquired on a Zeiss LSM 780 microscope equipped with a C-Apochromat 40x/1.20 W Korr M27, NA 1.2 objective and with ZEISS ZEN software (ZEN 2.3 SP1). Single cells not overlapping with any other cells at any structures were randomly selected and imaged according to the above-mentioned criteria. For F-/G-Actin quantification, images were acquired in a blinded way. Lasers with 488 and 561 nm excitation wavelengths were used and z -stacks with 0.708 μ m distance between z -planes were acquired. Data were analyzed as described previously.⁶¹ For co-localization analysis, 405 nm laser was used and combined according to the used secondary antibodies with the 488, 561 and 633 nm lasers, respectively. Z -stacks with the z -planes distance of 0.500 μ m were acquired and data were analyzed as described previously.⁶²

2.9 | Statistics and software

All statistical tests were performed with GraphPad Prism (Version 9.5.0(730), GraphPad Software, LLC). If applicable, statistical test used as well as numbers of biological and technical replicates are depicted in the figure legends.

Schematics were created as depicted using BioRender (<https://biorender.com/>, Toronto, Canada) with the agreement number NM24YEOIUL.

3 | RESULTS

3.1 | F-/G-Actin fractions are dysregulated in an SMA cell model

In a single cell analysis approach, we quantified F-/G-Actin fractions in NSC34 cells expressing different levels of the

full-length SMN protein (Figure 1A,B and Supplemental Figure S2), as described earlier.⁶⁰ The NSC34-Wildtype (SMN-WT) cells express SMN at a physiological protein level. The SMN-20% cells display a residual 20% expression of the full-length SMN protein compared to SMN-WT cells and are used as a cellular model of SMA. The SMN-0% cells harbor a complete knockout of the full-length SMN but express low levels of a truncated isoform, lacking exon 2B (SMN Δ 2B) (Figure 1A,B).^{60,63} F- and G-actin were visualized and quantified with Phalloidin-TRITC and DNaseI-Alexa488 staining (Figure 1C,D and Supplemental Figure S1), respectively. F-actin fractions were significantly upregulated in the SMN-20% and SMN-0% cells compared to wildtype cells (Figure 1C). No significant differences in F-actin fractions were measured between SMN-20% and SMN-0% cells (Figure 1C). However, upregulation of the F-actin fractions indicates a critical role for SMN in F-actin formation or stabilization. As F-actin remodeling plays a critical role in the regulation of cell morphology, especially in formation of typical neuronal structures such as dendrites and growth cones, we next analyzed cell morphology and correlated changes with F-actin fractions.

3.2 | Dysregulated actin dynamics leads to altered cell morphology

In a previous study, we have demonstrated that dysregulated actin dynamics leads to growth cone collapse in primary SMA motoneurons.⁵² The observed changes in F- and G-actin balance led to the hypothesis that SMN-20% and SMN-0% cells may display defects in cell shape and morphology. To test this hypothesis, we assessed single cells and quantified different morphological parameters. First, we quantified the total area of the cells and did not detect any significant difference between SMN-WT and SMN-20% cells (Figure 2A). SMN-0% cells showed a significant increase in cell area compared to SMN-WT or SMN-20% cells (Figure 2A). Degeneration of neurons results in more roundish cells since neurites degenerate and perikaryons increase in size. In contrast, activation of neurite outgrowth would lead to more thread-like shaped cells. Accordingly, quantification of cellular shape using the shape factor ($4\pi \cdot \text{area} / \text{perimeter}^2$) was conducted to quantitatively delineate neuronal morphology. A thread-like cellular shape would lead to a value very close to zero and a roundish shape close to one (Figure 2B). We could not detect any significant change in the shapes between the different cell clones. However, the distribution of the values shows a tendency of SMN-WT and SMN-0% cells being more thread-like shaped than the SMN-20% cells (Figure 2C). In addition, we aimed to clarify whether these

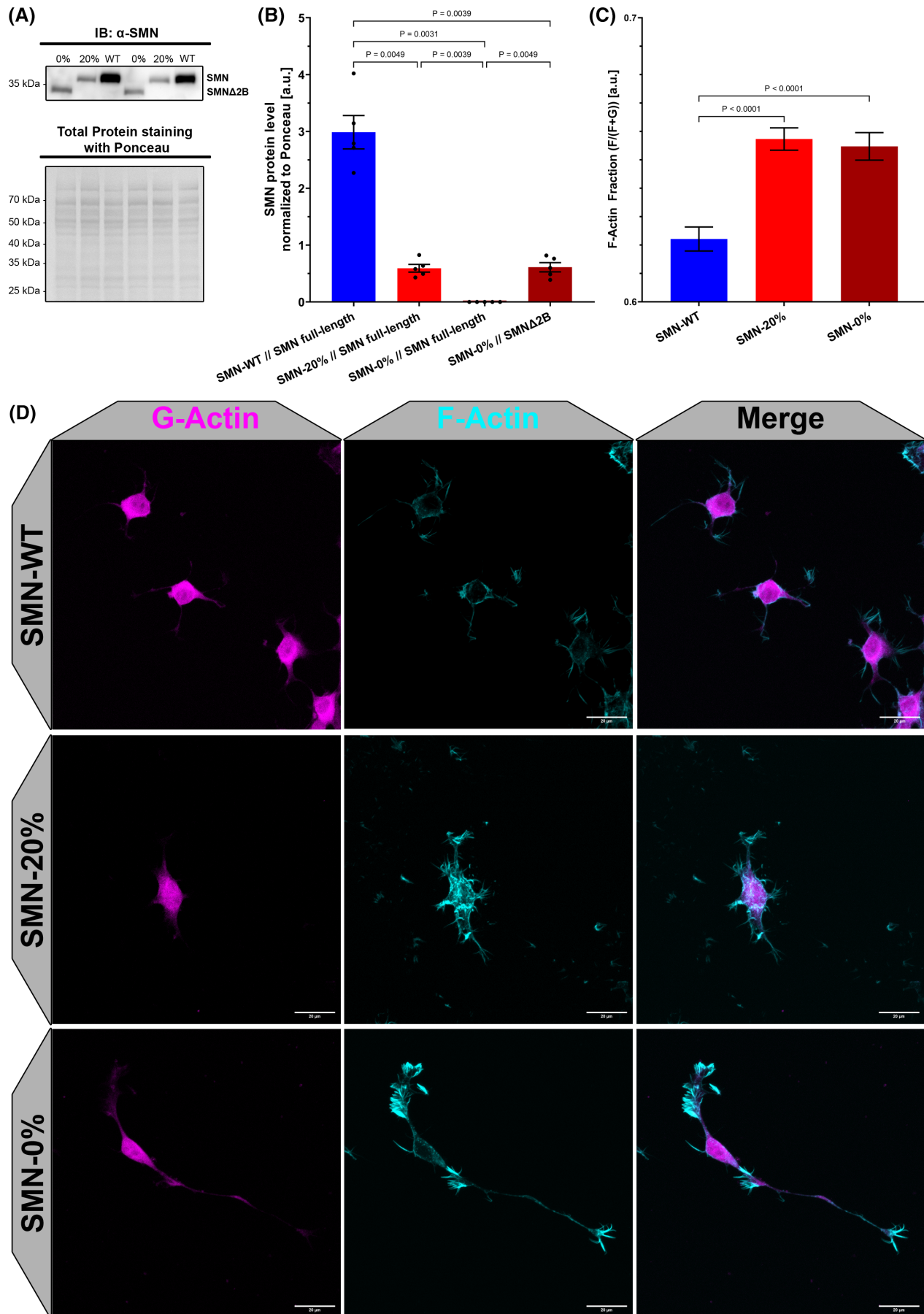


FIGURE 1 Legend on next page

FIGURE 1 F-/G-Actin fractions are altered in CRISPR/CAS modified NSC34 cells. (A) Representative Western Blot and Ponceau staining of endogenous SMN protein levels in SMN-WT, SMN-20% and SMN-0% cells. Ponceau staining was used for normalization of SMN levels. SMN-0% cells express the truncated SMN Δ 2B isoform lacking the Exon2B. (B) Quantification of residual SMN protein levels. Total protein per respective lane was used for normalization. For SMN-0% cells, SMN full-length expression was not measurable and set to zero. Expression level of truncated isoform SMN Δ 2B in SMN-0% cells was quantified additionally. $n = 5$ independent biological replicates, repeated measures (RM) one-way ANOVA, Geisser–Greenhouse correction: $**p < .005$ followed by Holm–Šidák’s multiple comparisons test: $**p < .005$, ns, not significant, Standard Error of Mean depicted. (C) Quantification of F-/G-Actin fractions in NSC34 single cells. Five different passages of cells per condition were stained in technical duplicates. Cells were imaged in a blinded way; quantification was done as described in Methods section. Single cell analysis was performed with a total number of cells quantified: N (SMN-WT) = 422, N (SMN-20%) = 442, N (SMN-0%) = 274. Mean F-Actin fraction for each cell-type: SMN-WT = 0.6221; SMN-20% = 0.6573; SMN-0% = 0.6547. Ordinary one-way ANOVA: $****p < .0001$ followed by Holm–Šidák’s multiple comparisons test: $****p < .0001$, Standard Error of Mean depicted. (D) Representative Maximum intensity projections of different NSC34 cells stained for G-Actin (magenta) and F-Actin (cyan). Scale bar = 20 μ m.

alterations are associated with changes in the F-/G-actin fractions. We correlated the F-actin fraction of each cell with its shape factor (Figure 2D–F). No correlation was found in the SMN-WT cells (Pearson $r = .01$) (Figure 2D). However, SMN-20% cells and SMN-0% cells showed weak correlations that are in opposite directions (SMN-20% cells: Pearson $r = .21$, SMN-0% cells: Pearson $r = -.21$) (Figure 2E,F). Increasing F-Actin fractions in SMN-20% cells were positively correlated with an increasing cell shape factor, indicating a shift towards more roundish cells. In contrast, increasing F-actin fractions in SMN-0% cells correlated with a decreasing cell shape factor representing more thread-like cells (Figure 2E,F). For differentiated neurons, a more thread-like shape is expected due to formation of neurites.

Neurite outgrowth relies on functional actin dynamics. To elucidate whether neurite outgrowth is dysregulated in our model, we performed a Sholl-analysis to quantify neurite parameters. Sholl-analyses provide information such as length and branching by calculating concentric circles around the center of the cell. The number of intersections of the neurites is calculated dependent on the distance from the center. Surprisingly, the SMN-0% cells showed a significant increase in the length of the longest process compared to SMN-WT or SMN-20% cells (Figure 2G). The integral of Sholl-curve, number of intersections plotted against distance from cell center, describes general differences between cell-types. Indeed, the integral of Sholl was higher for SMN-0% cells compared to SMN-WT and SMN-20% cells (Figure 2H,I). In a distance from 26.5 to 62.5 μ m from the cell center, we detected significantly more neurites in SMN-0% cells compared to SMN-WT and SMN-20% cells. The latter displayed the same mean number of intersections (Figure 2H,I). Moreover, the mean number of intersections in a radius closer to the cell center of SMN-0% cells was significantly decreased compared to SMN-WT and SMN-20% cells (Figure 2H). Again, we correlated the neurite lengths with F-actin fractions (Figure 2J–L). In SMN-WT cells, higher F-actin fractions correlated with neurite lengths only (Pearson $r = .22$) (Figure 2J).

SMN-20% (Pearson $r = .06$) (Figure 2K) and SMN-0% (Pearson $r = .12$) (Figure 2L) cells showed no correlation.

Taken together, we showed that functional actin dynamics relies on full-length SMN protein levels (Figure 1B,C). A shift in F-/G-actin fractions in SMN-depleted cells correlates with changes of cellular morphology (Figure 2). The SMN Δ 2B protein isoform expressed in SMN-0% cells has a comparable expression level as the residual full-length SMN protein in SMN-20% cells (Figure 1B). The SMN-20% cells showed a different morphology compared to SMN-0% cells. However, F-/G-actin fractions were similar (Figure 2). This implicates, that at the cellular level, the SMN-0% cells do not reflect the phenotype of SMN-20% cells. Neurite outgrowth in our model was not significantly altered between SMN-WT and SMN-20% cells (Figure 2G,H). Nevertheless, we detected a shift in the correlation of F-/G-actin fractions with neurite lengths in SMN-WT versus SMN-20% cells (Figure 2J,K). These results suggest an actin filament organization defect in SMN-depleted cells and, consequently, that SMN is a relevant regulatory element of actin dynamics. So far, SMN depletion was shown to alter the regulation of actin-binding proteins and upstream neurotrophic kinases leading to dysregulation of actin dynamics.^{44,52} Here, the results could also suggest a direct interaction of SMN and actin.

3.3 | The SMN protein and actin interact and co-localize with each other

To analyze whether SMN and actin interact directly with each other, we conducted co-immunoprecipitation, in vitro pulldown, and co-localization assays. Immunoprecipitation of SMN in SMN-WT cells and detection of actin revealed a strong signal. An unspecific immunoglobulin (IgG) control served as negative control and did not show any actin (Figure 3A). Vice versa, pulldown of actin in the SMN-WT cells showed a strong SMN signal (Figure 3A). This suggests a direct interaction of both

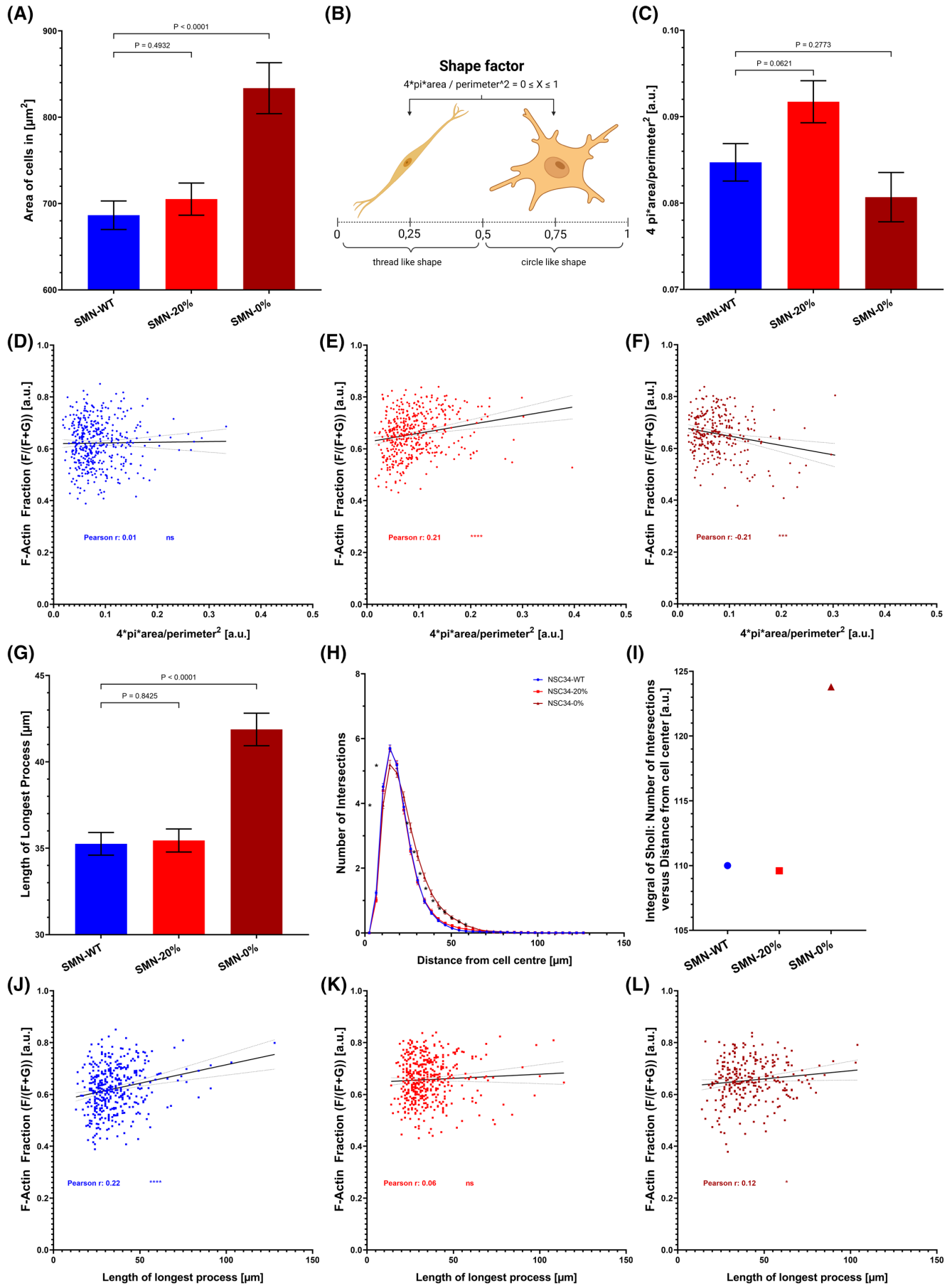


FIGURE 2 Legend on next page

FIGURE 2 Dysregulated F-/G-Actin fractions correlate with altered cellular morphology. (A) Quantification of total cell area per single cell. Mean area in μm^2 for each cell-type as depicted in graph: SMN-WT = $686 \pm \text{SEM}$; SMN-20% = $705 \pm \text{SEM}$; SMN-0% = $833 \pm \text{SEM}$. Ordinary one-way ANOVA: **** $p < .0001$ followed by Holm-Šidák's multiple comparisons test: **** $p < .0001$, ns, not significant, Standard Error of Mean (SEM) depicted. (B) The shape factor $4\pi \cdot \text{area}/\text{perimeter}^2$ was used to describe cell morphology. A shape factor closer to the value of 0 reflects a more thread like cell with 0 being a perfect thread. A value closer to 1 reflects a more circle like shape with a perfect circle with a value of 1. Created with BioRender. (C) Quantification of the shape factor $4\pi \cdot \text{area}/\text{perimeter}^2$ per single in different NSC34 cells. Mean shape factor for each cell-type: SMN-WT = $0.09 \pm \text{SEM}$; SMN-20% = $0.09 \pm \text{SEM}$; SMN-0% = $0.08 \pm \text{SEM}$. Ordinary one-way ANOVA: ** $p < .05$ followed by Holm-Šidák's multiple comparisons test: Ns = not significant, Standard Error of Mean (SEM) depicted. (D–F) Correlation of the F-Actin fraction of each cell with its shape factor separated per cell type. (D) SMN-WT show no correlation. Pearson $r = .014$, ns = not significant. (E) SMN-20% cells show a positive correlation between the F-Actin fraction and the shape factor. Pearson $r = .21$, **** $p < .0001$ (F) SMN-0% cells show a negative correlation between the F-Actin fraction and the shape factor. Pearson $r = -.21$, **** $p < .0005$. (G) Sholl-analysis was performed on single cells and mean length of longest process [μm] was compared between different cell types. SMN-WT = $35.3 \mu\text{m}$; SMN-20% = $35.5 \mu\text{m}$; SMN-0% = $41.9 \mu\text{m}$. Ordinary one-way ANOVA: **** $p < .0001$ followed by Holm-Šidák's multiple comparisons test: **** $p < .0001$, ns = not significant. (H) Mean number of intersections in distinct radii from the cell center were plotted for each cell type. SMN-WT and -20% cells do not differ in the number of intersections. However, -0% cells show decreased number of intersections close to the cell center and increased number of intersections in more distal regions. Two-way repeated measures (RM) ANOVA with Geisser–Greenhouse correction: **** $p < .0001$ followed by Tukey's multiple comparisons test: Significant differences in number of intersections at distinct radius from cell center between SMN-WT and SMN-0% as well as SMN-20% versus SMN-0% cells are marked with * in the graph. * $p < .01$ (I) Integral of all curves from (H) were calculated and plotted. SMN-0% cells show an increased integral reflecting the increased number of intersections. (J–L) Correlation of the F-Actin fraction of each cell with the length of the longest process of each cell. (J) SMN-WT show a positive correlation. Pearson $r = .22$, **** $p < .0001$. (K) SMN-20% cells show no correlation. Pearson $r = .06$, ns = not significant. (L) SMN-0% cells show a weak positive correlation. Pearson $r = .12$, * $p < .05$. (A, C, D–K) Total number of cells quantified in all depicted analyses: N (SMN-WT) = 422, N (SMN-20%) = 442, N (SMN-0%) = 274.

proteins at endogenous expressional levels. We repeated these pulldowns immunoprecipitations in the SMN-20% SMA cellular model. When endogenous SMN protein was significantly downregulated, pulldown of SMN did not show any actin (Figure 3B). However, enrichment of SMN by immunoprecipitation was successful even with significantly reduced SMN protein levels in SMN-20% cells (Supplemental Figure S3A,B). Furthermore, pulldown of actin still showed an SMN signal (Figure 3B), which indicates a reduced, yet abundant interaction of the remaining SMN with actin.

To further elucidate the specific interaction of SMN with either F- and G-actin, we stained F-/G-actin and endogenous SMN protein in SMN-WT and SMN-20% cells and performed quantitative co-localization analyses (Figure 4A,B). In SMN-WT cells, we could observe a positive SMN co-localization with F-actin as indicated by a Pearson coefficient larger than 0.5. Interestingly, SMN displayed a striking co-localization with G-actin, which indicates that SMN interacts with both F- and G-actin, but preferentially with the latter (Figure 4B). Reduced SMN levels in SMN-20% cells did not alter the co-localization of G-actin with the residual endogenous SMN protein (mean Pearson $r = .82$). However, the co-localization of F-actin with the remaining SMN was significantly increased (mean Pearson $r = .69$) compared to SMN-WT cells (Figure 4B). Furthermore, co-localization of G- and F-actin was significantly increased in SMN-20% cells compared to SMN-WT (Figure 4B). This finding is in agreement with the data showing increased F-/G-actin

fractions as measured in SMN-20% cells (Figure 1C), since increased co-localization of G- with F-actin might favor an increased F-actin formation. Taken together, endogenous SMN and actin co-immunoprecipitated in SMN-WT cells. This interaction is reduced in SMN-depleted cells which might be due to significantly reduced endogenous SMN protein levels. SMN co-localized with both, G- and F-actin but preferentially with G-actin (Figure 4). F-/G-actin fractions and G-/F-actin co-localization in SMN depleted cells were increased indicating more F-actin formation (Figures 1C and 4B). Additionally, co-localization of SMN with F-actin but not with G-actin was increased in SMA cells (Figure 4B). Since SMN interacts with G-actin via its transient binding to PFN2a, the shift of co-localization with F-actin in SMN-depleted cells implicates a PFN2a-independent interaction (Table 1, Graphical Abstract).

We have previously shown that the SMN wild-type protein directly interacts with the actin-binding protein profilin2 via its poly-L-proline (PLP) stretches. This interaction is transient and unlikely to be detected via co-immunoprecipitation. However, to rule out that SMN co-immunoprecipitates actin indirectly via profilin, we purified an SMN-GST fusion protein and actin, respectively, for an in vitro pulldown assay (Figure 4C). The SMN-GST fusion protein directly bound to F- but preferentially to G-actin (Figure 4C). Since G-actin tends to polymerize spontaneously, we performed additional experiments in the presence of Latrunculin B, an actin polymerization inhibitor, which allowed us to distinguish between F-actin and G-actin binding.⁶⁴ Our

results indicate that SMN has a higher binding affinity towards G-actin than to F-actin (Figure 4C). To confirm SMN is interacting with actin independently of binding to Pfn2a in our cellular model, we used a mutated SMN variant, the patient-derived single point mutant S230L. The S230L mutation closely localizes to the PLP domain of SMN resulting in a decreased SMN-PFN2a interaction.^{52,65–67} We expressed the SMN-S230L-Flag mutant in SMN-WT and SMN-20% cells to analyze the SMN-actin interaction. Anti-Flag staining revealed successful transfection and expression of this mutant in SMN-WT and SMN-20% cells, but with decreased intensity (Figure 5). This was caused by instability of the SMN-S230L-Flag mutant which resulted in a low protein expression (Figure 6A,B). Again, co-localization analyses of

SMN-Flag or SMN-S230L-Flag, respectively, with G- and F-actin were conducted (Figures 5 and 6C). Both proteins co-localized with F- and preferentially with G-actin comparable to endogenous SMN (Figure 6C). Importantly, this demonstrates that the disrupted profilin-interaction in the S230L mutant does not influence the SMN-actin co-localization pattern and indicates that S230L interacts with actin similar to the wild-type SMN i.e., co-localization of SMN with G-actin was higher than with F-actin (Figure 6C). This is supported by a prominent rescue effect on the G-/F-actin co-localization which was not significantly increased in SMN-20% cells compared to SMN-WT upon expression of both full-length SMN-Flag and SMN-S230L-Flag. This result indicates that the alteration of G-/F-actin co-localization does not

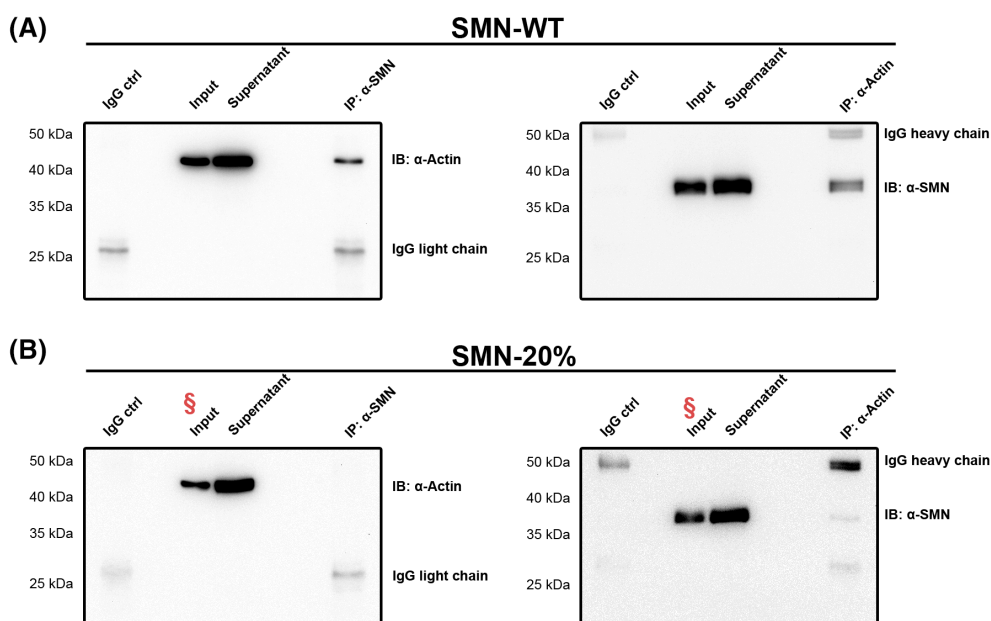
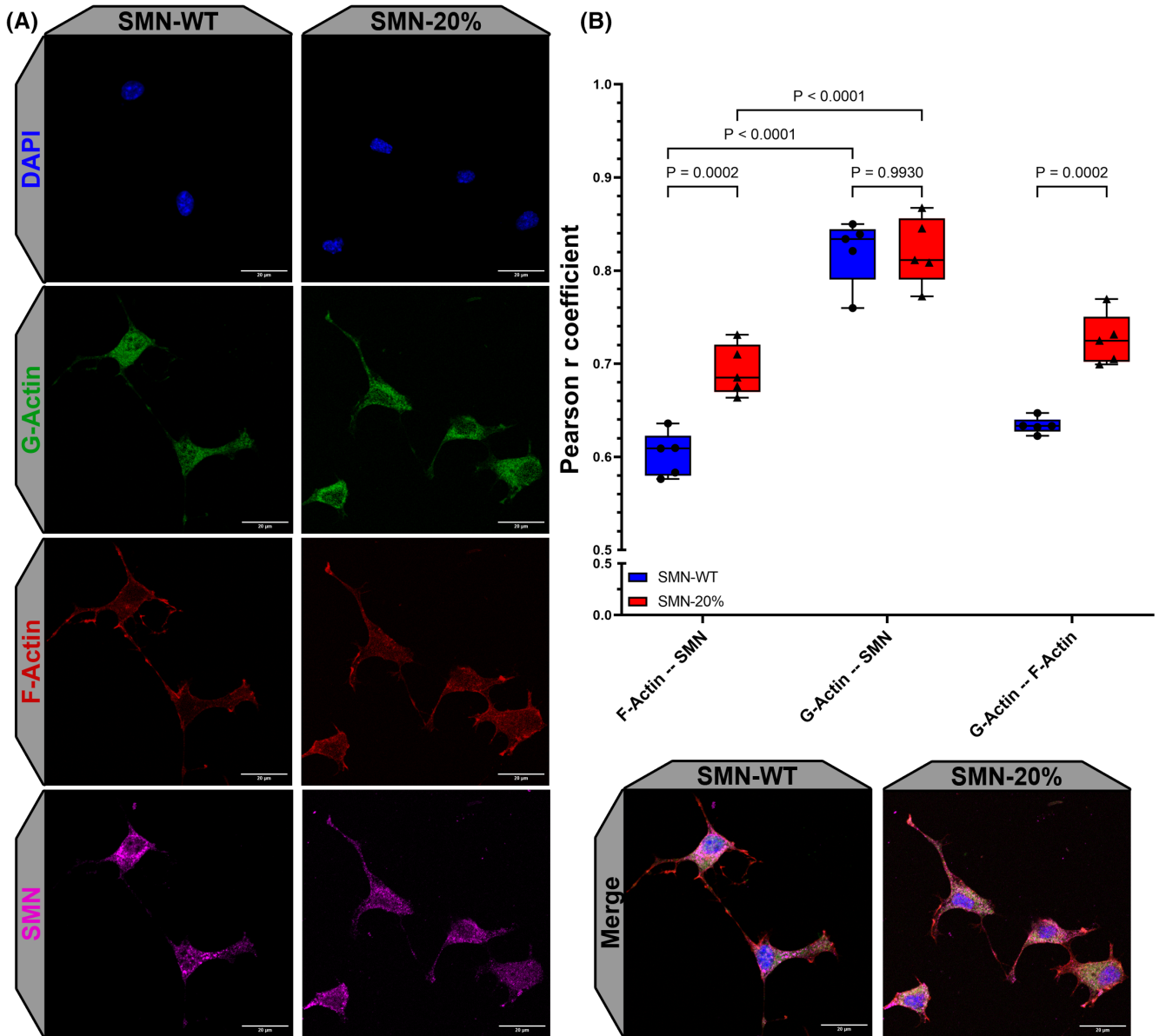


FIGURE 3 Co-Immunoprecipitation of endogenous SMN and Actin. Protein lysates of SMN-WT (A) and SMN-20% (B) cells were prepared as described in Methods section. Co-Immunoprecipitation assays were done with either α -SMN or α -Actin antibody, respectively. (A) In SMN-WT cells, SMN and Actin co-immunoprecipitate irrespectively whether SMN or Actin was pulled down. Input equals 5% of total protein amount used for immunoprecipitation. (B) In SMN-20% cells, we only detected interaction when Actin was immunoprecipitated and SMN was detected after Western-Blot analysis. § Since SMN protein expression is reduced to 20%, here the contrast was vastly increased compared to (A) to visualize all possible signals on membrane. Therefore, signal intensities of Input do not reflect knockdown situation. $n = 3$ biological independent replicates. IB, immuno-blot; IP: immunoprecipitation. Control blots are shown in Supplemental Figure S3.

FIGURE 4 Co-localization of endogenous SMN with F-/G-Actin in NSC34 cells. (A) Representative maximum projections of SMN-WT and SMN-20% cells stained for F-/G-Actin and endogenous SMN protein. Confocal images were acquired using a LSM 780 microscope. Five randomly chosen region of interests were acquired blinded for the genotype. Scale bar = 20 μ m. (B) Quantification of Pearson coefficient for co-localization as depicted. SMN-WT cells are depicted in blue, SMN-20% cells in red. p -values are depicted above graphs. Ordinary two-way ANOVA: **** $p < .0001$ for co-localization, followed by Holm-Šidák's multiple comparisons test: **** $p < .0001$, $p > .05$ = not significant, Standard Error of Mean (SEM) depicted, $n = 5$. (C) SMN-GST was purified and bound to Streptavidin beads. G-Actin, polymerized F-Actin were incubated with SMN-GST to analyze SMN binding to both Actin populations, F- & G-Actin, independently of profilin2a. To ensure specificity of the pull-down assay, negative controls (GST and G-Actin // GST and G-Actin + Latrunculin // GST and F-Actin // SMN-GST fusion construct only // Actin and Streptavidin beads only) were included. SMN bound strongly to G-, but also to F-Actin. Spontaneous actin polymerization was inhibited by adding Latrunculin. IB: Immuno-Blot. $n = 1$ independent biological replicate. Control blots are shown in Supplemental Figure S3.



(C) *in vitro* SMN-Actin pulldown

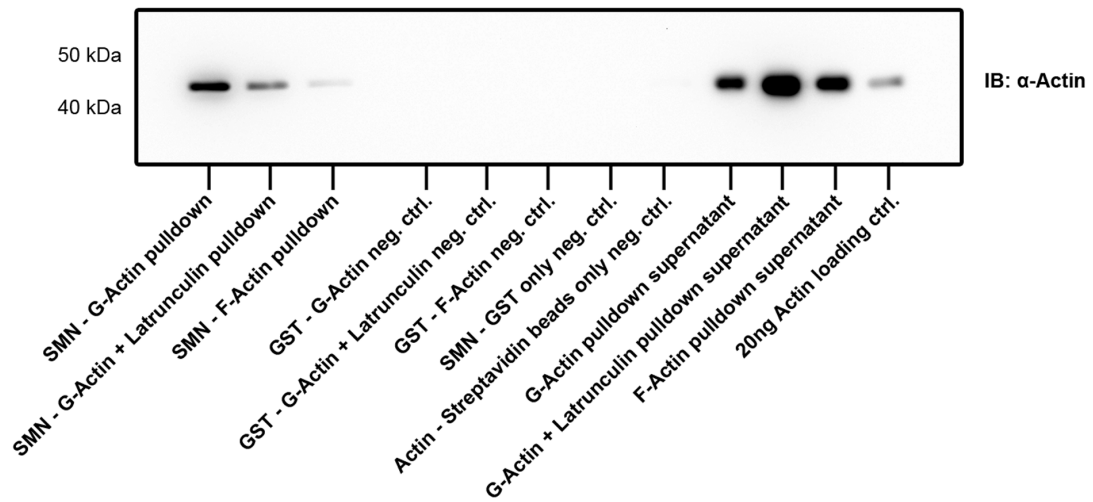


FIGURE 4 Legend on previous page

TABLE 1 SMN regulates actin dynamics and co-localizes with F- and G-actin.

	SMN-WT	SMN-20%	SMN-0%
SMN protein level	–	↓	No SMN full-length
F-/G-Actin fractions	–	↑	↑
Cell area	–	=	↑
Shape [thread-like or circle-like]	Thread-like	Thread-like	Thread-like
F-/G-Actin fractions versus shape	No correlation	Weak positive correlation	Weak negative correlation
Neurite length	–	–	↑
F-/G-Actin fractions versus neurite length	Weak positive correlation	No correlation	No correlation
SMN-Actin Co-immunoprecipitation	✓	↓	n.a.
F-Actin Co-localization SMN	✓	↑	n.a.
G-Actin Co-localization SMN	✓	=	n.a.
G-Actin Co-localization F-Actin	✓	↑	n.a.
SMN-Flag expression	✓	=	n.a.
F-Actin Co-localization SMN-Flag	✓	Tendency: ↗	n.a.
G-Actin Co-localization SMN-Flag	✓	Tendency: ↗	n.a.
G-Actin Co-localization F-Actin with background SMN-Flag expression	✓	=	n.a.
SMN-S230L-Flag expression	Very low	Very low	n.a.
F-Actin Co-localization SMN-S230L-Flag	= (compared to SMN-Flag in SMN-WT cells)	Tendency: ↘ (compared to SMN-Flag in SMN-WT cells)	n.a.
G-Actin Co-localization SMN-S230L-Flag	= (compared to SMN-Flag in SMN-WT cells)	Tendency: ↘ (compared to SMN-Flag in SMN-WT cells)	n.a.
G-Actin Co-localization F-Actin with background SMN-Flag expression	= (compared to SMN-Flag in SMN-WT cells)	=	n.a.

depend solely on PFN2a-binding to SMN, since both proteins partially rescued this alteration of co-localization. However, the expression of SMN-S230L-Flag reduced the level of co-localization of both G- and F-actin with SMN-S230L-Flag in SMN-20% cells but not in SMN-WT cells (Figure 6C). We assume that this effect is caused by

the loss of the SMN-PFN2a-actin population when using the S230L mutant. These findings support the hypothesis that SMN interacts with actin in two modes, independently and dependent of the actin-binding protein profilin2a. According to this model, cells comprise different populations: SMN-PFN2a-actin and SMN-actin,

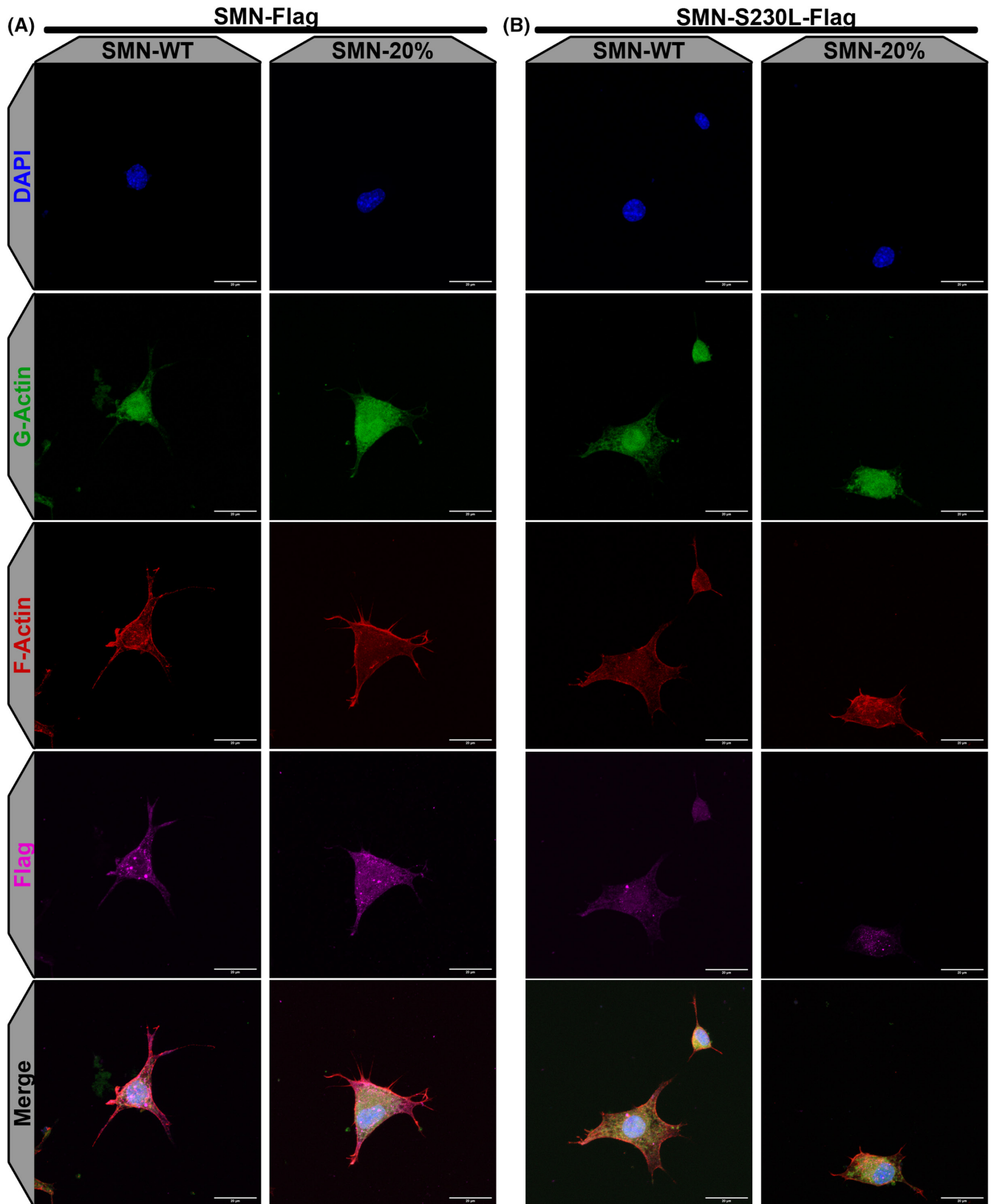


FIGURE 5 Co-localization of SMN with F-/G-Actin in NSC34 cells. SMN-WT and SMN-20% cells were transfected with either pCI-neo-SMN-Flag (A) or pCI-neo-SMN-S230L-Flag (B) constructs. All cells were stained for F-/G-Actin and with an anti-Flag antibody to assess co-localization of the Actin cytoskeleton with SMN-Flag or SMN-S230L-Flag protein. At six randomly chosen region of interest, confocal data stacks were acquired. Only criteria for selection were positive Flag staining. Representative Maximum intensity projections are depicted. Scale bar = 20 μm.

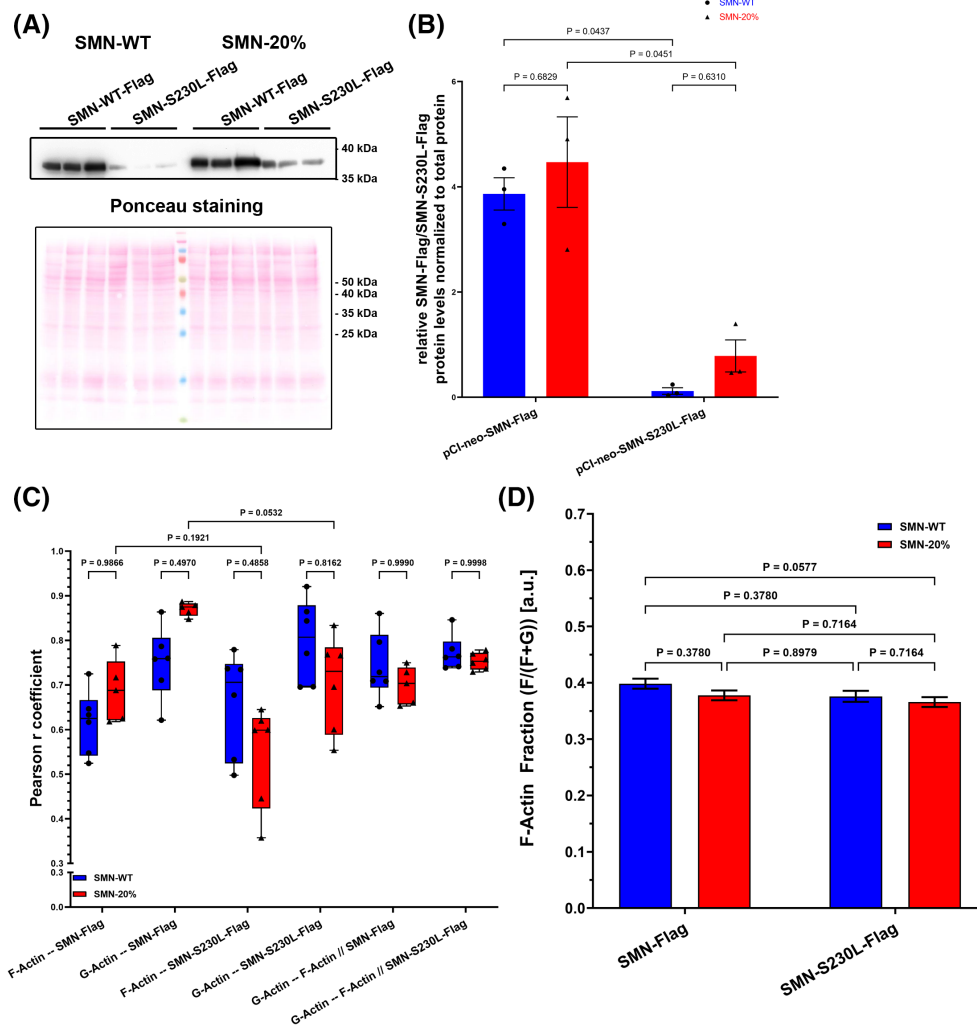


FIGURE 6 Co-localization of ectopically expressed SMN proteins with F-/G-Actin and quantification of F-/G-Actin fractions in NSC34 cells. (A) SMN-WT and SMN-20% cells were transfected with pCI-neo-SMN-Flag or pCI-neo-SMN-S230L-Flag. At DIV5, cells were lysed and protein lysates were used for SDS-Page and Western Blot analysis. Proteins were detected using an anti-Flag antibody to omit detection of endogenous SMN protein. Ponceau staining was used for normalization of signal intensity. (B) Relative SMN-Flag and SMN-S230L-Flag expression in SMN-WT (blue) or SMN-20% (red) cells. Signals were normalized to Ponceau staining. The full-length SMN-Flag protein is expressed in both, SMN-WT and SMN-20% cells. However, the SMN-S230L-Flag protein seems to be extremely unstable leading to a significantly reduced protein expression in both SMN-WT and SMN-20% cells. Repeated measures two-way ANOVA: $p = .0184$ for SMN construct followed by Tukey's multiple comparisons test: * for $p < .05$, $p > .05 =$ not significant, Standard Error of Mean (SEM) depicted, $n = 3$. (C) Quantification of Pearson coefficient for co-localization as depicted. SMN-WT cells are depicted in blue, SMN-20% cells in red. Note that G-/F-Actin co-localization was quantified in cells transfected with the SMN-Flag (G-Actin—F-Actin // SMN-Flag) and in cells transfected with SMN-S230L-Flag (G-Actin—F-Actin // SMN-S230L-Flag) to evaluate the impact of both proteins on G-/F-Actin co-localization. p -values are depicted above graphs. Ordinary two-way ANOVA: ** $p < .005$ for co-localization, followed by Holm-Šidák's multiple comparisons test: * $p < .05$, $p > .05 =$ not significant, Standard Error of Mean (SEM) depicted, $n = 6$. (D) Quantification of F-/G-Actin fractions in SMN-WT and SMN-20% cells transfected with SMN-Flag and SMN-S230L-Flag constructs. F-/G-Actin fractions in SMN-WT cells are depicted in blue and for SMN-20% cells in red. Furthermore, increased F-Actin fractions in SMN-20% were rescued with both SMN-Flag and SMN-S230L-Flag constructs. Single cell analysis with transfected cells only was performed for the following total number of cells: $N(\text{SMN-WT // SMN-Flag}) = 85$, $N(\text{SMN-WT // SMN-S230L-Flag}) = 67$, $N(\text{SMN-20% // SMN-Flag}) = 89$, $N(\text{SMN-20% // SMN-S230L-Flag}) = 82$. Mean F-Actin fractions for each condition: SMN-WT & SMN-Flag = 0.3985; SMN-WT and SMN-S230L-Flag = 0.3760; SMN-20% and SMN-Flag = 0.3777; SMN-20% and SMN-S230L-Flag = 0.3660. Ordinary two-way ANOVA: not-significant followed by Holm-Šidák's multiple comparisons test: Not significant for all comparisons. Standard Error of Mean (SEM) and p -values for Holm-Šidák's multiple comparison depicted.

and both are relevant for functional actin dynamics [Graphical Abstract] with both populations regulating each other. This hypothesis additionally implies that

increased F-/G-actin fractions in our SMA cellular model are rescued by ectopic expression of both, SMN-Flag and SMN-S230L-Flag constructs. Therefore, we quantified

F-/G-actin fractions in SMN-WT and SMN-20% cells transfected with SMN-Flag and SMN-S230L-Flag, respectively. Indeed, both constructs rescued the increased F-actin fractions in the SMN-20% cells (Figure 6D). We could not observe any differences comparing both constructs and cell types (Figure 6D).

In SMN-depleted cells, we showed hyperphosphorylation of PFN2a and dysregulation of actin dynamics.⁵² Consequently, PFN2a protein homeostasis becomes dysregulated and only a reduced population remains available for actin and SMN-actin regulation. Here, we showed that the SMN-actin population becomes increased in SMN-20% cells (Figure 6C). Restoration of SMN levels in SMN-20% cells cannot completely rescue SMN co-localization with F- and G-actin (Figures 5 and 6C) but rescues F-/G-actin fractions (Figure 6D).

3.4 | PFN2a co-localization with Gemin2 is altered in SMA

Previous studies showed that SMN and PFN2a co-localize in neurites and in SMN-positive nuclear bodies.^{52,56} Gemin2 and Sm proteins are major components of SMN complexes. However, Sm proteins are mainly found in the SMN-complex localizing to the nucleus.^{29–31,56,68,69} When PFN2a protein homeostasis becomes dysregulated in SMN-depleted cells, we would expect altered co-localization with Gemin2 and Sm proteins. Therefore, we stained for PFN2a, Gemin2 and Sm proteins in SMN-WT and SMN-20% cells to assess co-localization of these proteins (Figure 7).

PFN2a co-localized with Gemin2 and Sm proteins in both, SMN-WT and SMN-20% cells (Figure 7C). However, co-localization of PFN2a with Gemin2 was significantly downregulated in SMN-20% cells (Figure 7C). Co-localization of PFN2a with Sm proteins was not altered by reduced SMN-protein levels (Figure 7C). This indicates that cytoplasmic PFN2a, but not the nuclear localization becomes dysregulated.

4 | DISCUSSION

In this study, we analyzed the influence of SMN on actin dynamics at single-cell level and found an SMN-dependent imbalance in the F-/G-actin fractions. Motoneuron-like cells showed increased F-actin formation in SMN-depleted cells. These findings are consistent with a previous study of our group, in which we showed an increased F-/G-actin ratio in the growth cones of primary SMA mouse motoneurons causing growth cone collapse.⁵²

Previous studies showed that SMN-depleted cells display a deficit in neurite outgrowth, which is connected

to dysfunctional actin dynamics.^{42,43} Interestingly, we detected increased neurite outgrowth in the SMN-0% cells harboring a complete full-length SMN protein knockout (Figure 2G–I). This finding fits partially to a previous study in which we detected increased neurite length in NSC34 cells upon siRNA-mediated SMN knockdown.⁴⁴ However, no defect in neurite outgrowth was measurable in the SMN-20% cells, which more closely reflect SMN expression in SMA than the SMN-0% cells (Figure 2G–I). This difference might be explained by the cellular models used in those studies. Previously, rat adrenal pheochromocytoma (PC12) cells, which form long neurite-like structures upon stimulation with nerve growth factor (NGF), were used for measurement of neurite outgrowth.⁴² However, another explanation could be that SMN knockdown causes dysfunctional axonal pathfinding and branching leading to neuronal degeneration with no direct decrease in neurite outgrowth. This hypothesis is supported by a previous study in zebrafish, in which defects in neurite outgrowth were caused by dysfunctional axonal pathfinding and branching.⁷⁰ Our results in NSC34 cells and the study in zebrafish suggest an F-actin organizational defect, which does not induce a direct decrease in neurite outgrowth. However, alteration of neuronal morphology critically depends on actin dynamics. We quantitatively assessed morphological parameters such as cellular shape. Neurons are expected to be more thread-like due to formation of neurites and dendrites. This was true for all cell lines, SMN-WT, SMN-20% and SMN-0% (Figure 2C). However, increased F-/G-actin fractions correlated weakly with more roundish SMN-20% cells and more thread-like SMN-0% cells, respectively (Figure 2E,F). This result implies a F-actin organizational defect because no evident correlation was observed in SMN-WT cells (Figure 2D). This conclusion is supported by the data showing a correlation of neurite length with F-/G-actin fractions in SMN-WT cells only (Figure 2J–L).

SMN co-localizes with axonal fiber tracts in primary rat motoneurons⁷¹ and it is transported along filaments towards dendrites and synapses, e.g. neuromuscular junctions.⁷² Additionally, SMN was shown to transiently bind and regulate the small-actin binding protein PFN2a.^{51,52} Upon depletion of SMN, PFN2a protein homeostasis and actin dynamics become dysregulated.^{45,52,53} However, whether SMN stably binds to actin and directly regulates actin dynamics remained an open question. In the present study, we show that SMN interacts and co-localizes in vivo with F- and G-actin. We conducted co-immunoprecipitation assays and revealed that the SMN-actin interaction is reduced in SMA (Figure 3). Furthermore, co-localization and in vitro pulldown assays showed that SMN interacts with both F- but predominantly with G-actin (Figure 4B,C). Yet,

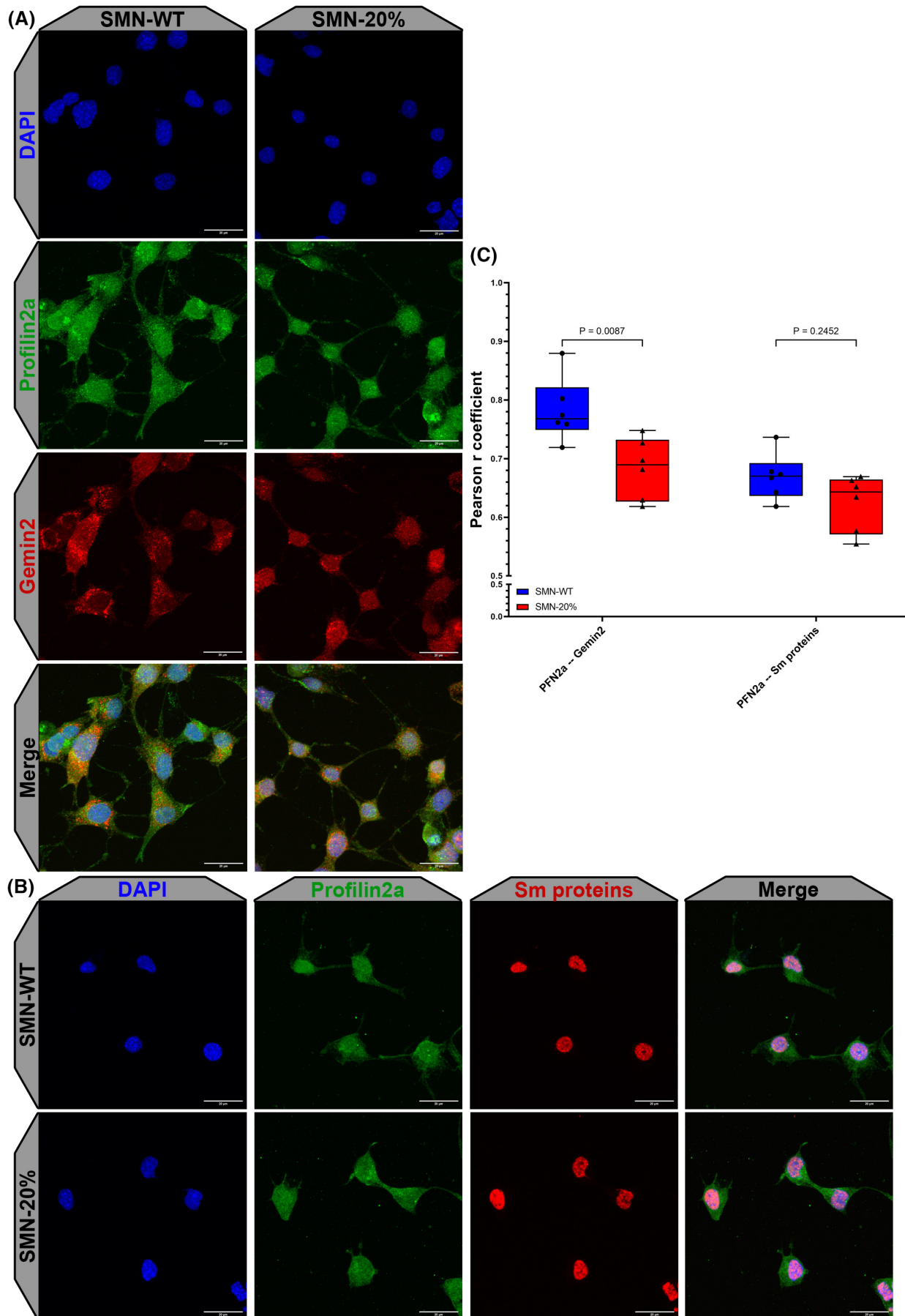


FIGURE 7 Legend on next page

FIGURE 7 Co-localization of Profilin2a with Gemin2 and Sm proteins. (A, B) SMN-WT cells and SMN-20% cells were stained for either Profilin2a and Gemin2 or Profilin2a and Sm proteins. Representative maximum intensity projections are shown. Confocal images at six randomly chosen region of interests were acquired. Scale bar = 20 μ m. (C) Quantification of Pearson coefficient for co-localization as depicted. SMN-WT cells are depicted in blue, SMN-20% cells in red. *p*-values are depicted above graphs. Ordinary two-way ANOVA: ***p* < .005 for the cell type, followed by Holm-Šidák's multiple comparisons test: **p* < .05, *p* > .05 = not significant, Standard Error of Mean (SEM) depicted, *n* = 6.

we detected a shift towards F-actin while there was no shift in G-actin-SMN co-localization upon SMN depletion (Figure 4B). This finding implies that SMN has a higher binding affinity towards G-actin and might stabilize actin filaments in SMA due to its increased F-actin co-localization. These findings are consistent with the results of an in vitro actin polymerization assay conducted in the presence of purified SMN.⁵⁶ Preincubation of actin with urea decreased the polymerization rate and led to decreased F-actin formation. However, in the presence of SMN and urea, the actin polymerization rate was partially rescued.⁵⁶ To elucidate whether this interaction and regulation of actin is independent of SMN-PFN2a-binding, we conducted an in vitro pull-down assay (Figure 4C) and expressed the SMN-S230L-Flag mutant in our NSC34 cells (Figures 5 and 6). We have previously shown, that SMN-S230L has a reduced capability to bind to PFN2a.⁵² First, expression of SMN-S230L-Flag showed a similar co-localization pattern compared to the SMN-Flag and endogenous SMN protein in SMN-WT cells (Figures 4B and 6C). Second, SMN-S230L-Flag and SMN-Flag both rescued the increased co-localization of G- and F-actin, which was prominent in SMN-20% cells (Figures 4B and 6C). Third, F- and G-actin both interacted directly with SMN-GST in the absence of profilin2a (Figure 4C). Fourth, SMN-S230L-Flag and SMN-Flag corrected increased F-/G-actin fractions upon ectopic expression in our SMA cellular model (Figure 6D). These findings support the hypothesis that SMN interacts with actin independently of PFN2a-binding. Therefore, we propose that two populations, both regulating actin dynamics, are present in neurons: SMN-PFN2a-actin and SMN-actin. In healthy neurons, these populations and their formation are mutually dependent in a tightly regulated equilibrium. Upon depletion or dysregulation of one of the essential factors such as SMN or PFN2a, the equilibrium is disrupted. In SMA, reduced SMN levels lead to hyperphosphorylation and sequestration of PFN2a by ROCK.⁵² This inhibits binding of PFN2a to actin. Subsequently, the SMN-PFN2a-actin population is decreased, and the SMN-F-actin population becomes more prominent i.e., increased co-localization, contributing to dysregulated actin dynamics.

Taken together, dysregulated PFN2a protein homeostasis, e.g. protein expression and hyperphosphorylation

as shown in SMA,^{45,52,53} contributes to neurodegeneration and dysregulated actin dynamics.⁷³ PFN2a co-localizes with SMN in different cellular compartments. In the nucleus, PFN2a and the SMN complex comprising Gemin2 and Sm proteins co-localize to SMN-positive nuclear bodies.^{29–31,51} In neurites and dendrites, SMN interacts with proteins of the SMN complex, however, in a different complex composition such as Gemin2 but not Sm proteins.^{56,68,69} We analyzed PFN2a co-localization with Gemin2 and Sm proteins to further elucidate the consequences of the altered interaction between PFN2a and SMN in SMA. Indeed, we detected significantly down-regulated PFN2a co-localization with Gemin2, but not with Sm proteins (Figure 7C). This supports the view that SMN depletion leads to a dysregulation of PFN2a protein homeostasis.

Interestingly, expression of the SMN-Flag construct in SMN-20% cells was not capable to fully rescue altered co-localization of F-actin with SMN. Furthermore, even co-localization of G-actin with SMN-Flag showed a tendency to be increased in SMN-20% cells (Figure 6C). In addition, the ectopic expression of SMN-Flag in SMN-WT and SMN-20% cells showed reduced total F-/G-actin fractions compared to endogenous expression (Figures 1C and 6D). This effect could be caused by two key factors: (I) hyperphosphorylation of PFN2a⁵² which is not rescued by restoration of SMN. Consequently, the equilibrium between SMN-actin and SMN-Profilin2a-actin populations is not fully restored. (II) SMN itself has a putative G-actin sequestering effect, therefore, SMN overexpression reduces F-actin polymerization. These results imply that SMN protein levels must be tightly regulated for functional actin organization. Furthermore, this indicates that dysregulated actin dynamics in SMA cannot be fully rescued by restoration of SMN protein levels alone. This underlines the need to further identify and characterize SMN-dependent and independent disease modifiers such as plastin3, neurocalcin delta (NCALD), senataxin or zinc finger protein ZPR1.^{27,34,74–79} Targeting those modifiers might help to correct dysregulated networks such as actin dynamics including neurotrophic signaling e.g., via plastin3 overexpression.^{53,74,77,79,80} Alternatively, some of these genes and proteins can regulate and stabilize SMN protein homeostasis e.g., ZPR1.³⁴ Therefore, understanding molecular consequences of SMN protein loss and

reconstitution is the key element for developing combinatorial treatment strategies.

AUTHOR CONTRIBUTIONS

Tobias Schüning, Andre Zeug, Peter Franz, Niko Hensel and Peter Claus conceived and designed research; Tobias Schüning, Andre Zeug, Katharina Strienke, Peter Franz performed research and acquired the data; Tobias Schüning, Andre Zeug, Katharina Strienke, Peter Franz, Peter Claus analyzed and interpreted the data; Tobias Schüning visualized the data. All authors were involved in drafting and revising the manuscript.

ACKNOWLEDGMENTS

We cordially thank Dr. Nora Detering (SMATHERIA gGmbH, Hannover, Germany) for providing the human SMN-Flag insert. Furthermore, we thank the members of the Claus group for discussions and suggestions. Moreover, we are grateful for funding by the Konrad-Adenauer Stiftung [to TS]. This work was supported by funds from Deutsche Forschungsgemeinschaft (DFG) through grant PO732 [to EP] and grant ZE994 [to AZ]. This work has been supported by the European Union's Horizon 2020 Marie Skłodowska-Curie Program (project 956185; SMABEYOND) [to PC]. Parts of this manuscript are included in the doctoral thesis of the first author (Tobias Schüning) published at the University of Veterinary Medicine Hannover (<https://nbn-resolving.org/urn:nbn:de:gbv:95-119041>) in 2023. Open Access funding enabled and organized by Projekt DEAL.

DISCLOSURES

The authors declare that they have no conflicts of interest with the contents of this article.

DATA AVAILABILITY STATEMENT

The original data that support the findings of this study are available upon request.

ORCID

Tobias Schüning  <https://orcid.org/0009-0000-7947-509X>

Andre Zeug  <https://orcid.org/0000-0001-9858-5841>

Katharina Strienke  <https://orcid.org/0009-0000-9419-961X>

Peter Franz  <https://orcid.org/0000-0001-9770-743X>

Georgios Tsiavaliaris  <https://orcid.org/0000-0002-5161-4884>

Niko Hensel  <https://orcid.org/0000-0002-1611-8906>

Gabriella Viero  <https://orcid.org/0000-0002-6755-285X>

Evgeni Ponimaskin  <https://orcid.org/0000-0002-4570-5130>

Peter Claus  <https://orcid.org/0000-0003-3824-9445>

REFERENCES

1. Crawford TO, Sladky JT, Hurko O, Besner-Johnston A, Kelley RI. Abnormal fatty acid metabolism in childhood spinal muscular atrophy. *Ann Neurol*. 1999;45(3):337-343. doi:10.1002/1531-8249(199903)45:3<337::aid-ana9>3.0.co;2-u
2. Vitte JM, Davoult B, Roblot N, et al. Deletion of murine Smn exon 7 directed to liver leads to severe defect of liver development associated with iron overload. *Am J Pathol*. 2004;165(5):1731-1741. doi:10.1016/S0002-9440(10)63428-1
3. Monani UR. Spinal muscular atrophy: a deficiency in a ubiquitous protein; a motor neuron-specific disease. *Neuron*. 2005;48(6):885-896. doi:10.1016/j.neuron.2005.12.001
4. Burghes AH, Beattie CE. Spinal muscular atrophy: why do low levels of survival motor neuron protein make motor neurons sick? *Nat Rev Neurosci*. 2009;10(8):597-609. doi:10.1038/nrn2670
5. Martinez-Hernandez R, Soler-Botija C, Also E, et al. The developmental pattern of myotubes in spinal muscular atrophy indicates prenatal delay of muscle maturation. *J Neuropathol Exp Neurol*. 2009;68(5):474-481. doi:10.1097/NEN.0b013e3181a10ea1
6. Hua Y, Sahashi K, Rigo F, et al. Peripheral SMN restoration is essential for long-term rescue of a severe spinal muscular atrophy mouse model. *Nature*. 2011;478(7367):123-126. doi:10.1038/nature10485
7. Hamilton G, Gillingwater TH. Spinal muscular atrophy: going beyond the motor neuron. *Trends Mol Med*. 2013;19(1):40-50. doi:10.1016/j.molmed.2012.11.002
8. Szunyogova E, Zhou H, Maxwell GK, et al. Survival motor neuron (SMN) protein is required for normal mouse liver development. *Sci Rep*. 2016;6:34635. doi:10.1038/srep34635
9. Wijngaarde CA, Blank AC, Stam M, Wadman RI, van den Berg LH, van der Pol WL. Cardiac pathology in spinal muscular atrophy: a systematic review. *Orphanet J Rare Dis*. 2017;12(1):67. doi:10.1186/s13023-017-0613-5
10. Nery FC, Siranosian JJ, Rosales I, et al. Impaired kidney structure and function in spinal muscular atrophy. *Neurol Genet*. 2019;5(5):e353. doi:10.1212/NXG.0000000000000353
11. Deguise MO, Baranello G, Mastella C, et al. Abnormal fatty acid metabolism is a core component of spinal muscular atrophy. *Ann Clin Transl Neurol*. 2019;6(8):1519-1532. doi:10.1002/acn3.50855
12. Allardyce H, Kuhn D, Hernandez-Gerez E, et al. Renal pathology in a mouse model of severe spinal muscular atrophy is associated with downregulation of glial cell-line derived neurotrophic factor (GDNF). *Hum Mol Genet*. 2020;29(14):2365-2378. doi:10.1093/hmg/ddaa126
13. Hensel N, Brickwedde H, Tsaknakis K, et al. Altered bone development with impaired cartilage formation precedes neuromuscular symptoms in spinal muscular atrophy. *Hum Mol Genet*. 2020;29(16):2662-2673. doi:10.1093/hmg/ddaa145
14. Lefebvre S, Burglen L, Reboullet S, et al. Identification and characterization of a spinal muscular atrophy-determining gene. *Cell*. 1995;80(1):155-165. doi:10.1016/0092-8674(95)90460-3
15. Lorson CL, Hahnen E, Androphy EJ, Wirth B. A single nucleotide in the SMN gene regulates splicing and is responsible for spinal muscular atrophy. *Proc Natl Acad Sci USA*. 1999;96(11):6307-6311. doi:10.1073/pnas.96.11.6307

16. Lefebvre S, Bulet P, Liu Q, et al. Correlation between severity and SMN protein level in spinal muscular atrophy. *Nat Genet.* 1997;16(3):265-269. doi:10.1038/ng0797-265
17. Lorson CL, Strasswimmer J, Yao JM, et al. SMN oligomerization defect correlates with spinal muscular atrophy severity. *Nat Genet.* 1998;19(1):63-66. doi:10.1038/ng0598-63
18. Lorson CL, Androphy EJ. An exonic enhancer is required for inclusion of an essential exon in the SMA-determining gene SMN. *Hum Mol Genet.* 2000;9(2):259-265. doi:10.1093/hmg/9.2.259
19. Feldkotter M, Schwarzer V, Wirth R, Wienker TF, Wirth B. Quantitative analyses of SMN1 and SMN2 based on real-time lightCycler PCR: fast and highly reliable carrier testing and prediction of severity of spinal muscular atrophy. *Am J Hum Genet.* 2002;70(2):358-368. doi:10.1086/338627
20. Wirth B, Brichta L, Schrank B, et al. Mildly affected patients with spinal muscular atrophy are partially protected by an increased SMN2 copy number. *Hum Genet.* 2006;119(4):422-428. doi:10.1007/s00439-006-0156-7
21. Dubowitz V. Very severe spinal muscular atrophy (SMA type 0): an expanding clinical phenotype. *Eur J Paediatr Neurol.* 1999;3(2):49-51. doi:10.1053/ejpn.1999.0181
22. D'Amico A, Mercuri E, Tiziano FD, Bertini E. Spinal muscular atrophy. *Orphanet J Rare Dis.* 2011;6:71. doi:10.1186/1750-1172-6-71
23. Kolb SJ, Kissel JT. Spinal muscular atrophy. *Neurol Clin.* 2015;33(4):831-846. doi:10.1016/j.ncl.2015.07.004
24. Ottesen EW. ISS-N1 makes the first FDA-approved drug for spinal muscular atrophy. *Transl Neurosci.* 2017;8:1-6. doi:10.1515/tnci-2017-0001
25. Ratni H, Ebeling M, Baird J, et al. Discovery of Risdiplam, a selective survival of motor neuron-2 (SMN2) gene splicing modifier for the treatment of spinal muscular atrophy (SMA). *J Med Chem.* 2018;61(15):6501-6517. doi:10.1021/acs.jmedchem.8b00741
26. Mendell JR, Al-Zaidy S, Shell R, et al. Single-dose gene-replacement therapy for spinal muscular atrophy. *N Engl J Med.* 2017;377(18):1713-1722. doi:10.1056/NEJMoa1706198
27. Hensel N, Kubinski S, Claus P. The need for SMN-independent treatments of spinal muscular atrophy (SMA) to complement SMN-enhancing drugs. *Front Neurol.* 2020;11:45. doi:10.3389/fneur.2020.00045
28. Gubitza AK, Feng W, Dreyfuss G. The SMN complex. *Exp Cell Res.* 2004;296(1):51-56. doi:10.1016/j.yexcr.2004.03.022
29. Liu Q, Fischer U, Wang F, Dreyfuss G. The spinal muscular atrophy disease gene product, SMN, and its associated protein SIP1 are in a complex with spliceosomal snRNP proteins. *Cell.* 1997;90(6):1013-1021. doi:10.1016/s0092-8674(00)80367-0
30. Fischer U, Liu Q, Dreyfuss G. The SMN-SIP1 complex has an essential role in spliceosomal snRNP biogenesis. *Cell.* 1997;90(6):1023-1029. doi:10.1016/s0092-8674(00)80368-2
31. Buhler D, Raker V, Luhrmann R, Fischer U. Essential role for the tudor domain of SMN in spliceosomal U snRNP assembly: implications for spinal muscular atrophy. *Hum Mol Genet.* 1999;8(13):2351-2357.
32. Pellizzoni L, Kataoka N, Charroux B, Dreyfuss G. A novel function for SMN, the spinal muscular atrophy disease gene product, in pre-mRNA splicing. *Cell.* 1998;95(5):615-624. doi:10.1016/s0092-8674(00)81632-3
33. Takizawa Y, Qing Y, Takaku M, et al. GEMIN2 promotes accumulation of RAD51 at double-strand breaks in homologous recombination. *Nucleic Acids Res.* 2010;38(15):5059-5074. doi:10.1093/nar/gkq271
34. Kannan A, Jiang X, He L, Ahmad S, Gangwani L. ZPR1 prevents R-loop accumulation, upregulates SMN2 expression and rescues spinal muscular atrophy. *Brain.* 2020;143(1):69-93. doi:10.1093/brain/awz373
35. Hensel N, Detering NT, Walter LM, Claus P. Resolution of pathogenic R-loops rescues motor neuron degeneration in spinal muscular atrophy. *Brain.* 2020;143(1):2-5. doi:10.1093/brain/awz394
36. Kariya S, Park GH, Maeno-Hikichi Y, et al. Reduced SMN protein impairs maturation of the neuromuscular junctions in mouse models of spinal muscular atrophy. *Hum Mol Genet.* 2008;17(16):2552-2569. doi:10.1093/hmg/ddn156
37. Tisdale S, Van Alstyne M, Simon CM, Mentis GZ, Pellizzoni L. SMN controls neuromuscular junction integrity through U7 snRNP. *Cell Rep.* 2022;40(12):111393. doi:10.1016/j.celrep.2022.111393
38. Imlach WL, Beck ES, Choi BJ, Lotti F, Pellizzoni L, McCabe BD. SMN is required for sensory-motor circuit function in Drosophila. *Cell.* 2012;151(2):427-439. doi:10.1016/j.cell.2012.09.011
39. Van Alstyne M, Simon CM, Sardi SP, Shihabuddin LS, Mentis GZ, Pellizzoni L. Dysregulation of Mdm2 and Mdm4 alternative splicing underlies motor neuron death in spinal muscular atrophy. *Genes Dev.* 2018;32(15-16):1045-1059. doi:10.1101/gad.316059.118
40. Simon CM, Van Alstyne M, Lotti F, et al. Stasimon contributes to the loss of sensory synapses and motor neuron death in a mouse model of spinal muscular atrophy. *Cell Rep.* 2019;29(12):3885-3901 e5. doi:10.1016/j.celrep.2019.11.058
41. Dimitriadi M, Derdowski A, Kalloo G, et al. Decreased function of survival motor neuron protein impairs endocytic pathways. *Proc Natl Acad Sci USA.* 2016;113(30):E4377-E4386. doi:10.1073/pnas.1600015113
42. van Bergeijk J, Rydel-Konecke K, Grothe C, Claus P. The spinal muscular atrophy gene product regulates neurite outgrowth: importance of the C terminus. *FASEB J.* 2007;21(7):1492-1502. doi:10.1096/fj.06-7136com
43. Simic G, Mladinov M, Seso Simic D, et al. Abnormal motoneuron migration, differentiation, and axon outgrowth in spinal muscular atrophy. *Acta Neuropathol.* 2008;115(3):313-326. doi:10.1007/s00401-007-0327-1
44. Hensel N, Stockbrugger I, Rademacher S, et al. Bilateral crosstalk of rho- and extracellular-signal-regulated-kinase (ERK) pathways is confined to an unidirectional mode in spinal muscular atrophy (SMA). *Cell Signal.* 2014;26(3):540-548. doi:10.1016/j.cellsig.2013.11.027
45. Bowerman M, Shafey D, Kothary R. Smn depletion alters profilin II expression and leads to upregulation of the RhoA/ROCK pathway and defects in neuronal integrity. *J Mol Neurosci.* 2007;32(2):120-131. doi:10.1007/s12031-007-0024-5
46. Hensel N, Rademacher S, Claus P. Chatting with the neighbors: crosstalk between Rho-kinase (ROCK) and other signaling pathways for treatment of neurological disorders. *Front Neurosci.* 2015;9:198. doi:10.3389/fnins.2015.00198
47. Hensel N, Baskal S, Walter LM, Brinkmann H, Gernert M, Claus P. ERK and ROCK functionally interact in a signaling network that is compensationally upregulated in

- spinal muscular atrophy. *Neurobiol Dis.* 2017;108:352-361. doi:10.1016/j.nbd.2017.09.005
48. Hensel N, Cieri F, Santonicola P, et al. Impairment of the neurotrophic signaling hub B-Raf contributes to motoneuron degeneration in spinal muscular atrophy. *Proc Natl Acad Sci USA.* 2021;118(18): e2007785118. doi:10.1073/pnas.2007785118
 49. Lee SH, Dominguez R. Regulation of actin cytoskeleton dynamics in cells. *Mol Cells.* 2010;29(4):311-325. doi:10.1007/s10059-010-0053-8
 50. Hensel N, Claus P. The actin cytoskeleton in SMA and ALS: how does it contribute to Motoneuron degeneration? *Neuroscientist.* 2018;24(1):54-72. doi:10.1177/1073858417705059
 51. Giesemann T, Rathke-Hartlieb S, Rothkegel M, et al. A role for polyproline motifs in the spinal muscular atrophy protein SMN. Profilins bind to and colocalize with smn in nuclear gems. *J Biol Chem.* 1999;274(53):37908-37914. doi:10.1074/jbc.274.53.37908
 52. Nölle A, Zeug A, van Bergeijk J, et al. The spinal muscular atrophy disease protein SMN is linked to the Rho-kinase pathway via profilin. *Hum Mol Genet.* 2011;20(24):4865-4878. doi:10.1093/hmg/ddr425
 53. Bowerman M, Anderson CL, Beauvais A, Boyl PP, Witke W, Kothary R. SMN, profilin Iia and plastin 3: a link between the deregulation of actin dynamics and SMA pathogenesis. *Mol Cell Neurosci.* 2009;42(1):66-74. doi:10.1016/j.mcn.2009.05.009
 54. Ferron F, Rebowski G, Lee SH, Dominguez R. Structural basis for the recruitment of profilin-actin complexes during filament elongation by Ena/VASP. *EMBO J.* 2007;26(21):4597-4606. doi:10.1038/sj.emboj.7601874
 55. Da Silva JS, Medina M, Zuliani C, Di Nardo A, Witke W, Dotti CG. RhoA/ROCK regulation of neuritogenesis via profilin Ii-mediated control of actin stability. *J Cell Biol.* 2003;162(7):1267-1279. doi:10.1083/jcb.200304021
 56. Sharma A, Lambrechts A, le Hao T, et al. A role for complexes of survival of motor neurons (SMN) protein with gemins and profilin in neurite-like cytoplasmic extensions of cultured nerve cells. *Exp Cell Res.* 2005;309(1):185-197. doi:10.1016/j.yexcr.2005.05.014
 57. Cashman NR, Durham HD, Blusztajn JK, et al. Neuroblastoma x spinal cord (NSC) hybrid cell lines resemble developing motor neurons. *Dev Dyn.* 1992;194(3):209-221. doi:10.1002/aja.1001940306
 58. Claus P, Bruns AF, Grothe C. Fibroblast growth factor-2(23) binds directly to the survival of motoneuron protein and is associated with small nuclear RNAs. *Biochem J.* 2004;384(Pt 3):559-565. doi:10.1042/BJ20040801
 59. Franz P, Gassl V, Topf A, Eckelmann L, Iorga B, Tsiavaliaris G. A thermophoresis-based biosensor for real-time detection of inorganic phosphate during enzymatic reactions. *Biosens Bioelectron.* 2020;169:112616. doi:10.1016/j.bios.2020.112616
 60. Bernabo P, Tebaldi T, Groen EJM, et al. In vivo Translatome profiling in spinal muscular atrophy reveals a role for SMN protein in ribosome biology. *Cell Rep.* 2017;21(4):953-965. doi:10.1016/j.celrep.2017.10.010
 61. Schill Y, Bijata M, Kopach O, et al. Serotonin 5-HT(4) receptor boosts functional maturation of dendritic spines via RhoA-dependent control of F-actin. *Commun Biol.* 2020;3(1):76. doi:10.1038/s42003-020-0791-x
 62. Muller FE, Schade SK, Cherkas V, et al. Serotonin receptor 4 regulates hippocampal astrocyte morphology and function. *Glia.* 2021;69(4):872-889. doi:10.1002/glia.23933
 63. Blatnik AJ, McGovern VL, Le TT, Iyer CC, Kaspar BK, Burghes AHM. Conditional deletion of SMN in cell culture identifies functional SMN alleles. *Hum Mol Genet.* 2020;29(21):3477-3492. doi:10.1093/hmg/ddaa229
 64. Bubb MR, Govindasamy L, Yarmola EG, et al. Polylysine induces an antiparallel actin dimer that nucleates filament assembly: crystal structure at 3.5-Å resolution. *J Biol Chem.* 2002;277(23):20999-21006. doi:10.1074/jbc.M201371200
 65. Detering NT, Schuning T, Hensel N, Claus P. The phospho-landscape of the survival of motoneuron protein (SMN) protein: relevance for spinal muscular atrophy (SMA). *Cell Mol Life Sci.* 2022;79(9):497. doi:10.1007/s00018-022-04522-9
 66. Qu YJ, Bai JL, Cao YY, et al. Mutation Spectrum of the survival of motor neuron 1 and functional analysis of variants in Chinese spinal muscular atrophy. *J Mol Diagn.* 2016;18(5):741-752. doi:10.1016/j.jmoldx.2016.05.004
 67. Yu-Jin Q, Juan D, Er-zhen L, et al. Subtle mutations in the SMN1 gene in Chinese patients with SMA: p.Arg288Met mutation causing SMN1 transcript exclusion of exon7. *BMC Med Genet.* 2012;13:86. doi:10.1186/1471-2350-13-86
 68. Rossoll W, Kroning AK, Ohndorf UM, Steegborn C, Jablonka S, Sendtner M. Specific interaction of Smn, the spinal muscular atrophy determining gene product, with hnRNP-R and gry-rbp/hnRNP-Q: a role for Smn in RNA processing in motor axons? *Hum Mol Genet.* 2002;11(1):93-105. doi:10.1093/hmg/11.1.93
 69. Jablonka S, Bandilla M, Wiese S, et al. Co-regulation of survival of motor neuron (SMN) protein and its interactor SIP1 during development and in spinal muscular atrophy. *Hum Mol Genet.* 2001;10(5):497-505. doi:10.1093/hmg/10.5.497
 70. McWhorter ML, Monani UR, Burghes AH, Beattie CE. Knockdown of the survival motor neuron (Smn) protein in zebrafish causes defects in motor axon outgrowth and pathfinding. *J Cell Biol.* 2003;162(5):919-931. doi:10.1083/jcb.200303168
 71. Pagliardini S, Giavazzi A, Setola V, et al. Subcellular localization and axonal transport of the survival motor neuron (SMN) protein in the developing rat spinal cord. *Hum Mol Genet.* 2000;9(1):47-56.
 72. Fan L, Simard LR. Survival motor neuron (SMN) protein: role in neurite outgrowth and neuromuscular maturation during neuronal differentiation and development. *Hum Mol Genet.* 2002;11(14):1605-1614. doi:10.1093/hmg/11.14.1605
 73. Walter LM, Franz P, Lindner R, Tsiavaliaris G, Hensel N, Claus P. Profilin2a-phosphorylation as a regulatory mechanism for actin dynamics. *FASEB J.* 2020;34(2):2147-2160. doi:10.1096/fj.201901883R
 74. Janzen E, Wolff L, Mendoza-Ferreira N, et al. PLS3 overexpression delays ataxia in Chp1 mutant mice. *Front Neurosci.* 2019;13:993. doi:10.3389/fnins.2019.00993
 75. Muinos-Buhl A, Rombo R, Janzen E, et al. Combinatorial ASO-mediated therapy with low dose SMN and the protective modifier Chp1 is not sufficient to ameliorate SMA pathology hallmarks. *Neurobiol Dis.* 2022;171:105795. doi:10.1016/j.nbd.2022.105795
 76. Muinos-Buhl A, Rombo R, Ling KK, et al. Long-term SMN- and Ncald-ASO combinatorial therapy in SMA mice and NCALD-ASO treatment in hiPSC-derived motor neurons show protective effects. *Int J Mol Sci.* 2023;24(4): 4198. doi:10.3390/ijms24044198
 77. Walsh MB, Janzen E, Wingrove E, et al. Genetic modifiers ameliorate endocytic and neuromuscular defects in a model of

- spinal muscular atrophy. *BMC Biol.* 2020;18(1):127. doi:[10.1186/s12915-020-00845-w](https://doi.org/10.1186/s12915-020-00845-w)
78. Wirth B, Karakaya M, Kye MJ, Mendoza-Ferreira N. Twenty-five years of spinal muscular atrophy research: from phenotype to genotype to therapy, and what comes next. *Annu Rev Genomics Hum Genet.* 2020;21:231-261. doi:[10.1146/annurev-genom-102319-103602](https://doi.org/10.1146/annurev-genom-102319-103602)
79. Wolff L, Strathmann EA, Muller I, et al. Plastin 3 in health and disease: a matter of balance. *Cell Mol Life Sci.* 2021;78(13):5275-5301. doi:[10.1007/s00018-021-03843-5](https://doi.org/10.1007/s00018-021-03843-5)
80. Hennlein L, Ghanawi H, Gerstner F, et al. Plastin 3 rescues cell surface translocation and activation of TrkB in spinal muscular atrophy. *J Cell Biol.* 2023;222(3): e202204113. doi:[10.1083/jcb.202204113](https://doi.org/10.1083/jcb.202204113)

SUPPORTING INFORMATION

Additional supporting information can be found online in the Supporting Information section at the end of this article.

How to cite this article: Schüning T, Zeug A, Strienke K, et al. The spinal muscular atrophy gene product regulates actin dynamics. *The FASEB Journal.* 2024;38:e70055. doi:[10.1096/fj.202300183R](https://doi.org/10.1096/fj.202300183R)